Table 2 Necropsy data

	Control	NTX-MI with vehicle	NTX-MI with aliskiren	NTX-MI with hydralazine	MI alone
Body weight (g)	24.96 ± 0.62	23.34 ± 0.45	23.60 ± 0.65	23.95 ± 0.34	26.23 ± 0.50*
Heart weight (mg)	116.6 ± 3.27*,#	137.38 ± 5.35	136.5 ± 2.88	135.17 ± 4.45	125.75 ± 5.93
H/B ratio (mg/g)	4.67 ± 0.08*,#	5.92 ± 0.31	5.80 ± 0.15	5.66 ± 0.21	4.70 ± 0.17*,#
Lung weight (mg)	135.8 ± 4.71	146 ± 4.16	135.83 ± 1.76	143.26 ± 3.13	127.44 ± 4.50
L/B ratio (mg/g)	5.44 ± ± 0.10*,‡	6.45 ± 0.12	5.69 ± 0.15*	6.07 ± 0.16	4.94 ± 0.07*,#,‡
LV weight (mg)	29.17 ± 3.57*	13.87 ± 2.19	27 ± 2.57*	24.92 ± 2.23	22.90 ± 0.99
RV weight (mg)	34.77 ± 1.19	32.33 ± 2.02	40.88 ± 1.75	34.26 ± 2.20	34.98 ± 2.73

*$P<0.05$ *vs* vehicle, #$P<0.05$ *vs* aliskiren, and ‡$P<0.05$ *vs* hydralazine.

Table 3 Pathological analysis

	Control	NTX-MI with vehicle	NTX-MI with aliskiren	NTX-MI with hydralazine	MI alone
Infarcted area (%)	0.00 ± 0.00#	21.55 ± 2.14	16.77 ± 1.52	20.28 ± 2.79	16.19 ± 1.66
LV thickness (mm)	1.36 ± 0.06#	0.43 ± 0.09*	0.75 ± 0.10**	0.45 ± 0.05	0.73 ± 0.07
Infarction length (mm)	0.00 ± 0.00#	6.3 ± 0.65*	5.58 ± 0.66	6.82 ± 0.97	3.26 ± 0.31
Septal wall thickness (mm)	1.25 ± 0.07	1.39 ± 0.14	1.17 ± 0.09	1.22 ± 0.12	1.48 ± 0.08
LV circumference (mm)	7.32 ± 0.34‡	12.11 ± 0.9*	8.89 ± 0.56**	11.47 ± 0.84	7.95 ± 0.43
Fibrosis in border zone (%)	0.00 ± 0.00	19.26 ± 2.41*	6.81 ± 2.00**	15.43 ± 3.04	4.74 ± 0.77

*$P<0.05$ *vs* control MI, **$P<0.05$ *vs* NTX-MI with vehicle, #$P<0.05$ *vs* each group, and ‡$P<0.05$ *vs* vehicle and hydralazine.

hypertrophy, however, cardiac function was comparable between the Tg and WT mice. (Table 2 and Supplementary Table 1). The creatinine level was not affected in the double-Tg mice compared with the age-matched WT mice (creatinine: WT 0.13 ± 0.01 mg/dl and double-Tg 0.18 ± 0.04 mg/dl). We induced MI in double-Tg and WT mice to analyze the effect of increasing RAS activation including renin in this model. We showed basal data of double-Tg mice in Supplementary Table 1. LAD ligation expanded remodeling at the LV anterior wall in the double-Tg mice compared with the WT mice. No Tg mice died after MI operation. MI hearts in the double-Tg mice showed impaired LVEF compared with the WT mice (Figure 5b). Collagen concentration from the cardiac ventricle was analyzed using hydroxyproline assay. MI hearts in double-Tg mice elevated collagen concentration compared with the WT + MI mice. Aliskiren treatment suppressed the concentration of collagen in double-Tg mice (Supplementary Figures 2C and D). The double-Tg mice showed increased deterioration of pathological myocardial remodeling after MI compared with WT + MI mice. We then examined levels of *ANP, collagen-type I, Nox2, Nox4,* and *MCP-1*. MI hearts in the double-Tg mice showed additionally elevated levels of *ANP, collagen-type I, Nox2, Nox4,* and *MCP-1* mRNA compared with the WT + MI mice. Aliskiren treatment suppressed BP increasing, cardiac dysfunction, LV remodeling, and inflammatory or oxidative factors in double-Tg mice compared with the non-treated double-Tg mice (Supplementary Figures 2E–I).

RAS Enhanced Oxidative Stress and *MCP-1* in *In Vitro*

Isolated cardiomyocytes were stimulated by murine plasma, and mRNA was collected 24 h after stimulation. Significantly, enhanced expression of *Nox2* mRNA levels was observed by NTX murine plasma stimulation compared with plasma from non-NTX mice. Plasma stimulation from aliskiren-treated NTX mice decreased expression of *Nox2* levels, whereas aliskiren-pretreated cardiomyocytes did not show altered mRNA levels. The *AT1*-deficient cardiomyocytes with stimulation of NTX mice plasma did not show increased *Nox2* levels (Figures 5a and b).

Plasma from NTX mice elevated expression of *Nox2* and *MCP-1* in primary mononuclear cells. Although plasma from aliskiren-treated mice did not alter these levels, aliskiren pretreated mononuclear cells showed significantly suppressed *Nox2* and *MCP-1* levels (Figures 5c and e). *AT1*-deficient mononuclear cells did not have suppressed *Nox2* and *MCP-1* expression, but aliskiren-treated mononuclear cells showed markedly suppressed expression of these factors compared with the NTX plasma-treated group (Figures 5d and f).

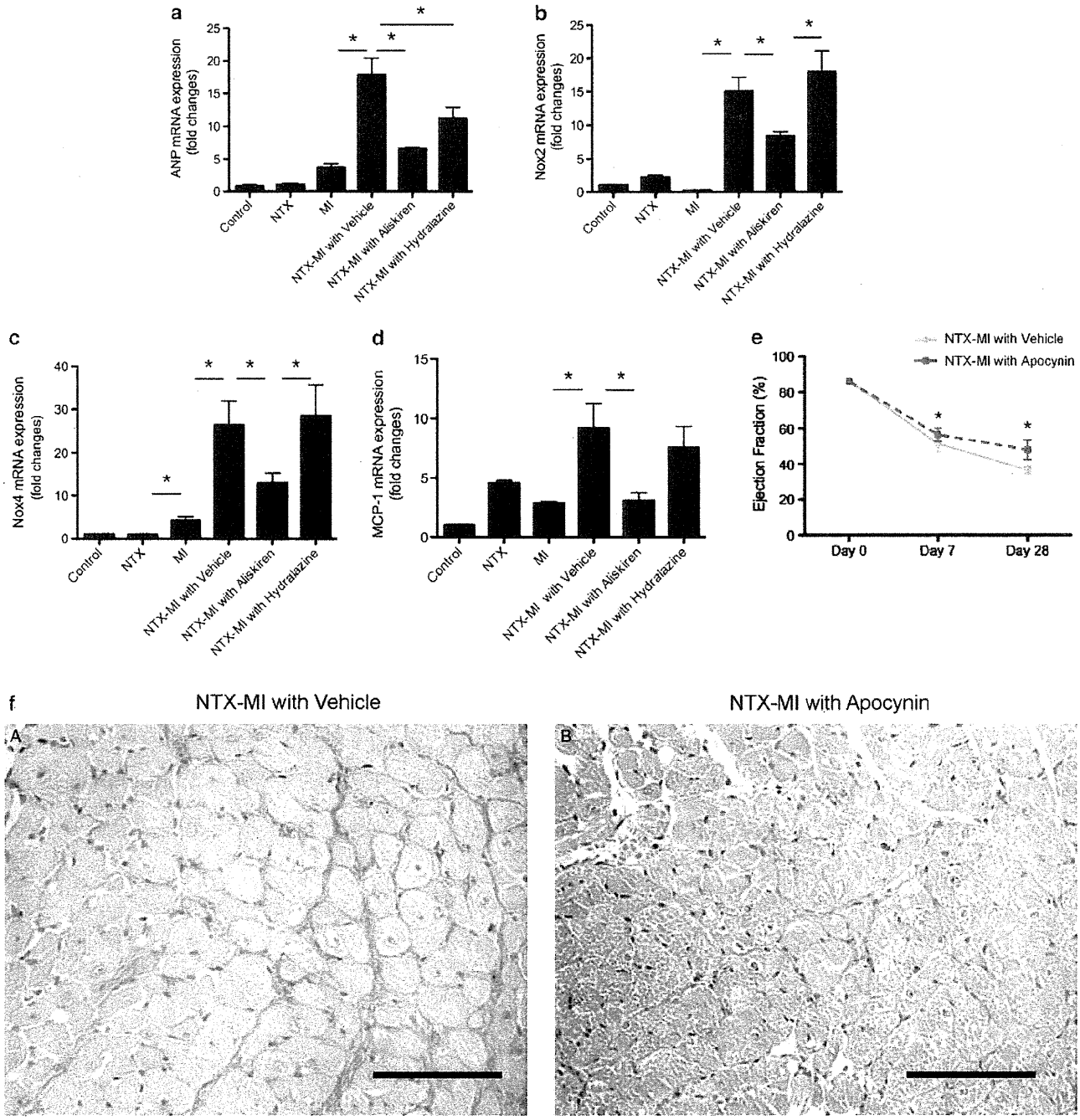

Figure 4 NTX (5/6 nephrectomy) enhanced *ANP*, oxidative stress, and monocytes chemoattractant protein (*MCP*)-*1* in myocardial ischemia (MI). Real-time (RT) PCR. We performed RT-PCR to analyze the expression of *ANP* (**a**), oxidative stresses (**b** and **c**) and *MCP-1* (**d**) in hearts from MI with NTX mice. $^*P<0.05$. (**e**) Representative left ventricular ejection fraction analysis of MI hearts with NTX. Mice were administrated apocynin (red line; $n=6$) or vehicle (blue line; $n=8$). (**f**) Representative light micrograph of apocynin-treated hearts from MI with NTX mice. $^*P<0.05$ *vs* vehicle.

DISCUSSION

In this study, we investigated the pathophysiology of ventricular remodeling after MI associated with renal failure. RAS activation by renal failure augmented myocardial remodeling, expression of inflammatory factors, and oxidative stress. Double-Tg mice showed myocardial remodeling and *Nox2* and *Nox4* elevation comparable to those of WT MI mice with NTX. In addition, a Nox inhibitor attenuated LV remodeling in MI plus NTX mice. We revealed that upregulated *Nox* induced by RAS

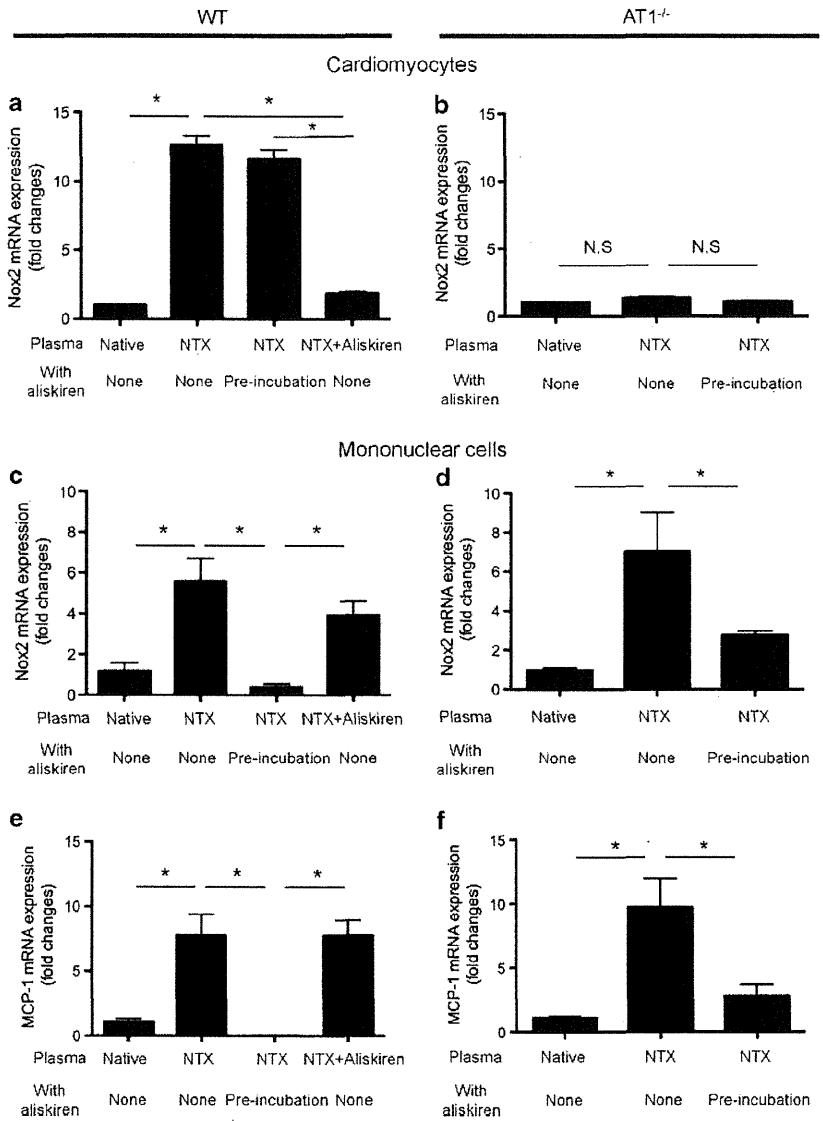

Figure 5 Renin–angiotensin system enhanced oxidative stress and monocytes chemoattractant protein (*MCP)-1* in *in vitro*. Cardiomyocytes were isolated from wild type (WT) (**a**) or *AT1* KO (**b**) and stimulated by murine plasma. (**a**) Representative real-time PCR data detecting the expression of *Nox2*. (**b**) Nox2 levels in *AT1*-deficient cardiomyocytes with stimulation of 5/6 nephrectomy (NTX) plasma. Mononuclear cells were isolated from WT (**c** and **e**) or *AT1* KO (**d** and **f**) and stimulated by the specified plasma. $^*P < 0.05$; NS, not significant.

stimulation has a pivotal role in the development of myocardial remodeling associated with renal dysfunction in this type IV cardiorenal syndrome (or chronic renocardiac symdrome) model.

It is known that oxidative stress, which results in cell damage, is increased in various cardiovascular diseases. The Nox protein family consists of well-known factors that characterize ROS-generating systems. Nox2 and Nox4 can also be activated by a number of stimuli, such as RAS, inflammatory cytokines, sheer stress, or hypoxia. Recent studies indicate that similar Nox systems are present in a wide variety of cells. Nox2 and Nox4 are known to be expressed in cardiomyocytes and fibroblasts and may potentially contribute to adverse remodeling. Previous studies showed that *Nox2*$^{-/-}$ reduced LV remodeling after aortic constriction or MI, suggesting that Nox2 exerted specific effects on the extracellular matrix.[22] Nox4 is known to be a key contributor in converting fibroblasts to myofibroblasts, which are a main contributor to cardiac fibrosis.[23] Nox4 overexpression in cardiomyocytes induces apoptosis resulting in expanded myocardial remodeling.[24] Therefore, elevated myocardial levels of Nox in NTX mice deteriorated MI-induced cardiac collagen synthesis and ventricular remodeling. We demonstrated that the MI plus NTX hearts showed upregulation of *Nox2* and *Nox4* compared with the MI plus non-NTX hearts. Moreover,

in vitro studies revealed that stimulation of plasma from NTX mice enhanced *Nox2* expression from WT cardiomyocytes, but not *AT1*-deficient cells. These results suggest that Nox expression was increased through the AT1 pathway and resulted in deteriorated myocardial remodeling through collagen synthesis.

MCP-1 is well known to be contributor to the development of LV remodeling following MI. The reduction against MCP-1 and the receptor suppress LV remodeling in MI models.[25,26] Our data, therefore, suggest that MCP-1 may have contributed to the development of LV remodeling in this model. Nox2 and MCP-1 were upregulated in mononuclear cells stimulated with NTX plasma or with NTX plus aliskiren plasma. However, cells stimulated with NTX that were pretreated with aliskiren did not show upregulation of these factors. Pre-treatment of aliskiren inhibits renin activation and Ang II expression, but does not have an inhibitory effect on already-produced Ang II. These results indicate that MCP-1 expression was not increased through the AT1 pathway. A previous study showed that renin deficiency of macrophage or aliskiren-reduced macrophage adhesion to endothelial cells resulted in suppression of atherosclerosis in mice.[8] Our data may indicate that aliskiren has a direct role on the anti-inflammatory effect through inactivation of macrophages. However, the underlying mechanism is unknown, and further investigation is needed to determine the effect of aliskiren on LV remodeling in $AT1^{-/-}$ mice and the mechanism of aliskiren action on monocytes.

This study demonstrated that NTX deteriorated MI-induced LV remodeling through RAS activation. Oxidative stresses such as increased Nox2, Nox4, and MCP-1 induced the activation of RAS. These proteins are known as key factors contributing to the development of LV remodeling through enhanced interstitial fibrosis and inflammation. These results suggested that the increase of inflammatory response affected development following MI. Aliskiren suppressed these factors and improved LV function and remodeling. Therefore, further investigation is needed to determine the clinical usefulness of RAS inhibition on cardiorenal syndrome. Interestingly, upregulation of cardiac AT1a receptor was evident after NTX in mice, and *in vitro* study showed a lack of AT1a receptor benefit on oxidative stress. This data suggest that AT1 blockers may also benefit the cardiac remodeling caused by MI plus CKD.

Our data showed that aliskiren treatment improved cardiac remodeling and dysfunction in NTX-MI mice without alteration of renal function. However, creatinine is imperfect in mice as a measure of renal function. We need further investigation using more solid methods to analyze the renal function.

In conclusion, RAS activation has a pivotal role in adverse MI-induced myocardial remodeling associated with renal failure, and aliskiren treatment improved the myocardial remodeling and suppressed the expression of oxidative stress and inflammatory factors in this cardiorenal models. Aliskiren treatment may be a new methodological approach about patients with cardiorenal syndrome.

Supplementary Information accompanies the paper on the Laboratory Investigation website (http://www.laboratoryinvestigation.org)

ACKNOWLEDGEMENTS

We especially thank Ms Noriko Tamura and Ms Yasuko Matsuda for their excellent technical assistance. This study was supported by the Japan Heart Foundation Young Investigator's Research Grant, a grant of the Research Fellow of the Japan Society for the Promotion of Science; Yokohama Research Grant from Research Foundation for Pharmaceutical Sciences; Takeda Science Foundation; and Suzuken Memorial Foundation.

DISCLOSURE/CONFLICT OF INTEREST

The authors declare no conflict interest.

1. Go AS, Chertow GM, Fan D, *et al.* Chronic kidney disease and the risks of death, cardiovascular events, and hospitalization. N Engl J Med 2004;351:1296–1305.
2. Virzì GM, Corradi V, Panagiotou A, *et al.* ADPKD: prototype of cardiorenal syndrome type 4. Int J Nephrol 2010;2011:490795.
3. McCullough P. Prevention of cardiorenal syndromes. Contrib Nephrol 2010;165:101–111.
4. McCullough PA. Cardiorenal syndromes: pathophysiology to prevention. Int J Nephrol 2011;2011:762590.
5. McCullough PA, Ahmad A. Cardiorenal syndromes. World J Cardiol 2011;3:1–9.
6. Strauss M, Hall A. Angiotensin receptor blockers may increase risk of myocardial infarction: unraveling the ARB-MI paradox. Circulation 2006;114:838–854.
7. Wood JM, Maibaum J, Rahuel J, *et al.* Structure-based design of aliskiren, a novel orally effective renin inhibitor. Biochem Biophys Res Commun 2003;308:698–705.
8. Lu H, Rateri DL, Feldman DL, *et al.* Renin inhibition reduces hypercholesterolemia-induced atherosclerosis in mice. J Clin Invest 2008;118:984–993.
9. Fisher ND, Jan Danser AH, Nussberger J, *et al.* Renal and hormonal responses to direct renin inhibition with aliskiren in healthy humans. Circulation 2008;117:3199–3205.
10. Solomon SD, Shin SH, Shah A, *et al.* Effect of the direct renin inhibitor aliskiren on left ventricular remodelling following myocardial infarction with systolic dysfunction. Eur Heart J 2011;32:1227–1234.
11. Westermann D, Riad A, Lettau O, *et al.* Renin inhibition improves cardiac function and remodeling after myocardial infarction independent of blood pressure. Hypertension 2008;52:1068–1075.
12. Burney BO, Kalaitzidis RG, Bakris GL. Novel therapies of diabetic nephropathy. Curr Opin Nephrol Hypertens 2009;18:107–111.
13. Parving HH, Brenner BM, McMurray JJ, *et al.* Aliskiren Trial in Type 2 Diabetes Using Cardio-Renal Endpoints (ALTITUDE): rationale and study design. Nephrol Dial Transplant 2009;24:1663–1671.
14. Fukamizu A, Sugimura K, Takimoto E, *et al.* Chimeric renin-angiotensin system demonstrates sustained increase in blood pressure of transgenic mice carrying both human renin and human angiotensinogen genes. J Biol Chem 1993;268:11617–11621.
15. Sugaya T, Nishimatsu S, Tanimoto K, *et al.* Angiotensin II type 1a receptor-deficient mice with hypotension and hyperreninemia. J Biol Chem 1995;270:18719–18722.
16. Tapia E, Franco M, Sánchez-Lozada L, *et al.* Mycophenolate mofetil prevents arteriolopathy and renal injury in subtotal ablation despite persistent hypertension. Kidney Int 2003;63:994–1002.
17. Shimazaki M, Nakamura K, Kii I, *et al.* Periostin is essential for cardiac healing after acute myocardial infarction. J Exp Med 2008;205:295–303.
18. Harraz MM, Marden JJ, Zhou W, *et al.* SOD1 mutations disrupt redox-sensitive Rac regulation of NADPH oxidase in a familial ALS model. J Clin Invest 2008;118:659–670.

19. Ogawa M, Suzuki J, Hishikari K, *et al.* Clarithromycin attenuates acute and chronic rejection via matrix metalloproteinase suppression in murine cardiac transplantation. J Am Coll Cardiol 2008;51: 1977–1985.
20. Reddy GK, Enwemeka CS. A simplified method for the analysis of hydroxyproline in biological tissues. Clin Biochem 1996;29: 225–229.
21. Ogawa M, Suzuki J, Kosuge H, *et al.* The mechanism of anti-inflammatory effects of prostaglandin E2 receptor 4 activation in murine cardiac transplantation. Transplantation 2009;87:1645–1653.
22. Looi YH, Grieve DJ, Siva A, *et al.* Involvement of Nox2 NADPH oxidase in adverse cardiac remodeling after myocardial infarction. Hypertension 2008;51:319–325.
23. Cucoranu I, Clempus R, Dikalova A, *et al.* NAD(P)H oxidase 4 mediates transforming growth factor-beta1-induced differentiation of cardiac fibroblasts into myofibroblasts. Circ Res 2005;97:900–907.
24. Ago T, Kuroda J, Pain J, *et al.* Upregulation of Nox4 by hypertrophic stimuli promotes apoptosis and mitochondrial dysfunction in cardiac myocytes. Circ Res 2010;106:1253–1264.
25. Hayashidani S, Tsutsui H, Shiomi T, *et al.* Anti-monocyte chemoattractant protein-1 gene therapy attenuates left ventricular remodeling and failure after experimental myocardial infarction. Circulation 2003;108:2134–2140.
26. Kaikita K, Hayasaki T, Okuma T, *et al.* Targeted deletion of CC chemokine receptor 2 attenuates left ventricular remodeling after experimental myocardial infarction. Am J Pathol 2004;165:439–447.

FEBS Open Bio 2 (2012) 145–150

FEBS openbio

journal homepage: www.elsevier.com/locate/febsopenbio

The manner in which DNA is packaged with TFAM has an impact on transcription activation and inhibition

Ryo Furukawa [a,1], Yuma Yamada [a,1], Yuichi Matsushima [b], Yu-ichi Goto [b], Hideyoshi Harashima [a,*]

[a] Laboratory for Molecular Design of Pharmaceutics, Faculty of Pharmaceutical Sciences, Hokkaido University, Kita-12, Nishi-6, Kita-ku, Sapporo 060-0812, Japan
[b] Department of Mental Retardation and Birth Defect Research, National Institute of Neuroscience, National Center of Neurology and Psychiatry, 4-1-1 Ogawahigashi, Kodaira, Tokyo 187-8502, Japan

ARTICLE INFO

Article history:
Received 9 May 2012
Revised 7 June 2012
Accepted 7 June 2012

Keywords:
Mitochondria
Mitochondrial transcription factor A (TFAM)
DNA packaging
Mitochondrial DNA (mtDNA)
Mitochondrial transcription

ABSTRACT

For successful mitochondrial transgene expression, an optimal packaging exogenous DNA is an important issue. We report herein on the effects of DNA packaged with mitochondrial transcription factor A (TFAM), which packages mitochondrial DNA (mtDNA), on the transcription process. Our initial findings indicated that the transcription of the TFAM/DNA complex was activated, when the complex was formed at an optimal ratio. We also found that TFAM has a significant advantage over protamine, a nuclear DNA packaging protein, from the viewpoint of transcription efficiency. This result indicates that TFAM can be useful packaging protein for exogenous DNA to achieve mitochondrial transgene expression.

1. Introduction

It has been reported that mutations and defects in the mitochondrial genome (mtDNA) can form the basis for a variety of human diseases [1,2]. Therefore, mitochondrial gene therapy and diagnosis would be expected to have substantial medical benefits. Mitochondrial transgene expression represents an attractive methodology for achieving such an innovative medical goal. However, successful examples of mitochondrial transgene expression have not been reported to date. On the other hand, many reports have appeared describing the use of a variety of applications for nuclear transgene expression, including cationic liposomes, cell-penetrating peptides, polycations, etc. [3]. The formation of nanoparticles between plasmid DNA (pDNA) and polycations have been extensively investigated by many researchers, because it is known that the manner in which pDNA is packaged with polycations has a substantial effect on gene expression [4,5]. Protamine is well known as a nuclear DNA condenser with a high transfection activity [6,7].

mtDNA is packaged with specific core proteins in a complex referred to as a mitochondrial nucleoid, which has been implicated, not only in replication and transcription but also in the maintenance of mtDNA [8–12]. Mitochondrial transcription factor A (TFAM), one of the major components of nucleoids [8,13], was initially identified as a factor that activates transcription on heavy and light strand mtDNA promoters (HSP and LSP) via sequence-specific binding [14–17]. TFAM also binds DNA non-specifically, a property that is essential for mtDNA packaging to play a crucial role in mtDNA maintenance [18–21]. The expression levels of TFAM and mtDNA are sufficiently interactive that the knockdown of TFAM results in mtDNA depletion, and a reduction in mtDNA copy number results in the degradation of TFAM [22,23]. Thus, TFAM largely contributes to mtDNA maintenance and would be expected to affect the replication and transcription.

Based on previous reports, we predicted that TFAM represents a potentially optimal DNA condenser for mitochondrial transgene expression. To validate this prediction, we compared DNA complexes produced using TFAM and protamine in terms of their physicochemical properties and transcription efficiency. We first prepared DNA complexes with TFAM and protamine at various molar ratios, and evaluated their physicochemical properties. We then evaluated the extent to which transcription was affected by the conformation of DNA packaged with DNA condensers using T7 RNA polymerase, an enzyme that is homologous to mitochondrial RNA polymerase [24,25]. We also compared the transcription efficiency of long circular DNA (pDNA, 6445 bp) and short linear DNA (1324 bp), to examine how the conformation in different-structured DNA packaged with TFAM affected transcription.

* Corresponding author. Fax: +81 11 706 4879.
E-mail address: harasima@pharm.hokudai.ac.jp (H. Harashima).
[1] These authors contributed equally to this work.

2211-5463/$36.00 © 2012 Federation of European Biochemical Societies. Published by Elsevier B.V. All rights reserved.
http://dx.doi.org/10.1016/j.fob.2012.06.001

2. Material and methods

2.1. Chemicals and materials

Protamine was purchased from Calbiochem (Darmstadt, Germany). T7 RNA polymerase, ribonuclease inhibitor and SYBR Green 2 were purchased from Takara (Shiga, Japan). The pTriEx-3 Neo vector (6445 bp) was obtained from Novagen (Madison, WI, USA). pDNA was purified using a Qiagen EndoFree Plasmid Mega Kit (Qiagen GmbH, Hilden, Germany). Ribonucleoside 5′-triphosphates were from GE Healthcare Bio-Sciences (Piscataway, NJ, USA). For the preparation of short linear DNA (1324 bp), pDNA was digested by *Tth111*I and *Xba*I, and subjected to agarose gel electrophoresis. Short linear DNA (1324 bp) was then extracted and purified using a QIAquick Gel extraction kit (Qiagen GmbH).

2.2. Purification of Recombinant TFAM

A fragment of human TFAM, corresponding to residues 43–246 (NCBI NP_003192) was amplified by PCR using the following pair of primers; 5′-ggggcatatgtcatctgtcttggcaagttg-3′ (forward) and 5′-ggggctcgagtctacttttaacactcctca-3′ (reverse). N-terminal protein region was reported to be mitochondrial targeting signal [26], and was, therefore, removed from our construct. To express human TFAM in *Escherichia coli*, the PCR fragment was cloned into pET-28a (Novagen) that had been cleaved with *Nde*I and *Xho*I. Bacterial cells harboring the plasmid were grown in LB medium containing 100 mg/L kanamycin, and expression was induced by treatment with 1 mM isopropylthiogalactoside. The N-terminal His tag was utilized for nickel-nitrilotriacetic acid affinity purification of the recombinant human TFAM according to the manufacturer's instructions (Qiagen GmbH). The purified protein was finally dialyzed against a buffer containing 10 mM Tris–HCl, pH 7.4, 150 mM NaCl, 1 mM dithiothreitol, and 20% glycerol. Protein concentrations were determined using a BCA protein assay kit (Pierce, Rockford, IL, USA).The purified protein was analyzed by SDS–PAGE to confirm that the recombinant human TFAM was purely prepared (Fig. S1).

2.3. Preparation of TFAM/DNA complex and protamine/DNA complex

For preparation of the DNA complex, DNA and TFAM (or protamine) solutions at various molar ratios were mixed in 10 mM HEPES buffer (pH 7.4) and the preparations then incubated at 25 °C for 30 min. Dynamic light scattering (DLS) was employed to determine the hydrodynamic diameters of the complexes in the suspension (Zetasizer Nano ZS; Malvern Instruments, Herrenberg, Germany). The ζ-average diameter (mean diameter) was calculated from a cumulants analysis based on the intensity of the scattered light. The ζ-potential, an indicator of surface potential, was determined electrophoretically using laser doppler velocimetry (Zetasizer Nano ZS).

2.4. Electrophoretic mobility shift assay of TFAM/DNA complex and protamine/DNA complex

To evaluate the packaging of DNA, TFAM/pDNA complex and protamine/pDNA complex were subjected to agarose gel electrophoresis before and after treatment with the polyanion preparation. The samples were incubated for 30 min at 25 °C with a polyanion, *i.e.*, a 1 mg/ml solution of poly (L-aspartic acid) (pAsp), to release the pDNA. A 0.1 μg sample of pDNA was subjected to electrophoresis. Electrophoresis was performed on a 1% agarose gel in TAE (40 mM Tris–HCl, 40 mM acetic acid, 1 mM EDTA, pH 8.0) at 100 V for 30 min. The gel was stained with EtBr and analyzed by ImageQuant LAS 4000 (GE Healthcare Bio-Sciences).

2.5. In vitro transcription assay

Transcription efficiencies of TFAM/DNA complex and protamine/DNA complex were evaluated by in vitro transcription assay using T7 RNA Polymerase as described below. DNA complexes containing pDNA (30 fmol) or short linear DNA (60 fmol) were incubated with T7 RNA Polymerase (17 U) at 37 °C for 2 h, in a reaction mixture (5.5 μL) containing incubation buffer (40 mM Tris–HCl, pH 8.0, 8 mM $MgCl_2$, 2.0 mM spermidine, 5.0 mM dithiothreitol), 1.0 mM ribonuclease inhibitor and the four ribonucleoside 5′-triphosphates (2 mM each). The reaction was terminated by the addition of 14.5 μL of blocking buffer (29.6 mM Mops, pH 7.0, 7.4 mM sodium acetate, 1.5 mM EDTA, 18.5% formaldehyde, 74.1% formamide) and then incubated at 65 °C for 15 min. The reaction mixtures were analyzed by 18% formaldehyde–1% agarose gel electrophoresis and stained with SYBR Green 2. Fluorograms were obtained with an ImageQuant LAS 4000 to evaluate transcription efficiency. Transcription efficiency was calculated as follows;

Transcription efficiency = intensity of the transcript band from samples/intensity of the transcript band from naked DNA.

2.6. Investigation of transcription inhibition by ultrafiltration and in vitro transcription assay

pDNA were packaged with TFAM at various molar ratios, and the resulting complexes were then subjected to ultrafiltration to remove unbound TFAM using Amicon Ultra Centrifugal Filters (14,000*g*, 25 °C,15 min). An in vitro transcription assay before and after ultrafiltration were performed, and as result, electrophoresis gel data of transcripts after in vitro transcription reactions were obtained (Fig. 4A). Relative transcription values were calculated as follows, the transcription efficiency of samples was normalized by maximum transfection efficiency among the samples (Fig. 4B).

3. Results

3.1. Physicochemical characteristics of TFAM/DNA complex and protamine/DNA complex

We first prepared pDNA complexes using several different molar ratios of pDNA (circular DNA, 6445 bp) and TFAM, or protamine that is a nuclear DNA packaging protein, which is a polycationic peptide rich in arginine residues [27]. Their particle sizes and ζ potentials are summarized in Fig. 1. The particle sizes of the pDNA complexes became smaller with increasing molar ratio in the case of both TFAM and protamine (Fig. 1A), however, major differences were observed in the case of ζ potentials (Fig. 1B). In the case of protamine/pDNA complex, as the molar ratio increased, negatively charged particles were converted into positively charged particles, with diameters of ~100 nm (Fig. 1, open diamonds). On the other hand, negatively charged particles were formed when TFAM packaged pDNA, and no positively charged ones were observed (Fig. 1, closed diamonds). These results suggest that DNA packaging between TFAM and protamine occur in a different manner.

3.2. Investigation of the stabilities of TFAM/DNA complex and protamine/DNA complex

We evaluated the stability of TFAM/pDNA complex and the protamine/pDNA complex by means of an electrophoretic mobility shift assay (Fig. 2). In this experiment, pDNA packaged with TFAM or protamine at various molar ratios, and the pDNA complexes were subjected to gel electrophoresis before and after treatment

with a counter polyanion (pAsp). A fluorescent band is observed by emitted as the result of EtBr intercalating with pDNA, when pDNA is released from the complex or is loosely packaged with TFAM (or protamine).

As shown in Fig. 2A, TFAM/pDNA complexes were detected by EtBr at any molar ratio in the absence of pAsp, although their mobilities were shifted to shorter values with increasing molar ratio (Fig. 2A, lanes 1–6). We also observed a similar tendency in the electrophoretic mobility shift of pDNA after pAsp treatment (Fig. 2A, lanes 7–12). On the other hand, the stability of the pDNA complex formed with protamine was quite different from that formed with TFAM (Fig. 2B). Protamine/pDNA complexes formed at molar ratios of 500 or more were undetectable by EtBr in the absence of pAsp (Fig. 2B, lanes 5 and 6), suggesting that pDNA is tightly packaged at high molar ratios. We also observed the release of pDNA from the protamine/pDNA complex after pAsp treatment (Fig. 2B, lanes 7–12), suggesting that electrostatic interactions between pDNA and protamine are major contributors to the packaging pDNA.

3.3. Comparison of the transcription efficiencies between TFAM/DNA complex and protamine/DNA complex

We examined the issue of how transcription efficiency was affected by the conformation of the pDNA packaged with TFAM (Fig. 3A). Transcription efficiency was estimated by using T7 RNA polymerase, an enzyme that is homologous to mitochondrial RNA polymerase [24,25]. The transcription from pDNA packaged with TFAM was activated in the optimal molar ratio, and an approximate twofold increase in transcription efficiency was found compared to the naked pDNA (Fig. 3A, closed diamonds). We also observed a decrease in the transcription efficiencies, when pDNA was packaged with TFAM at molar ratios of 500 and more. On the other hand, in the case of protamine, no activation of transcription was observed when pDNA was packaged at any molar ratio, and the transcription was progressively inhibited with increasing molar ratio (Fig. 3A, open diamonds).

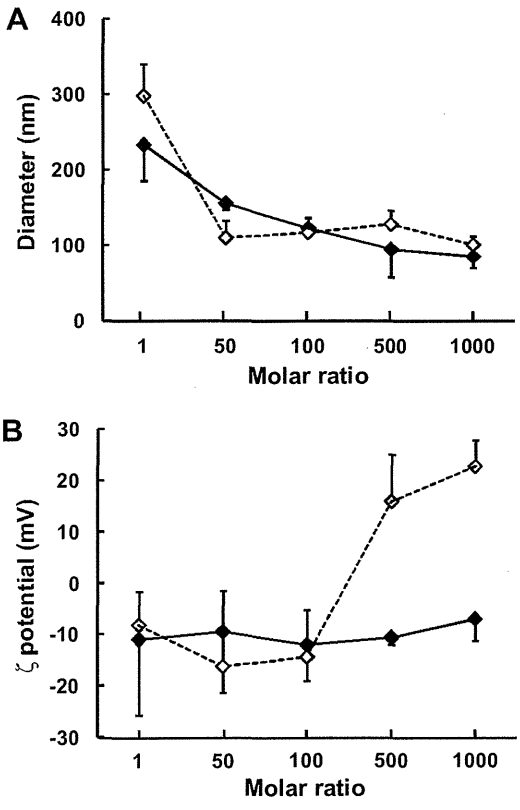

Fig. 1. Characteristics of pDNA packaged with TFAM or protamine. pDNA were packaged with TFAM (closed symbols) and protamine (open symbols) at various molar ratios, and their diameters (A) and ζ potentials (B) were then measured. Data are presented as the mean ± SD ($n = 3$).

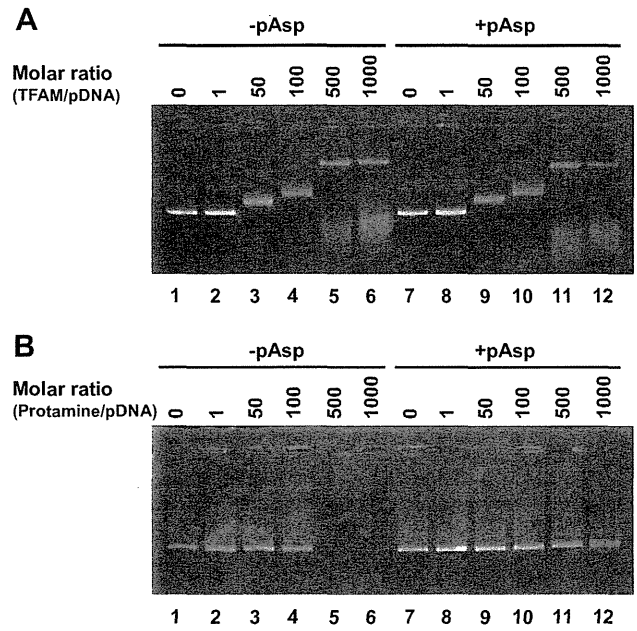

Fig. 2. Electrophoretic mobility shift assay of pDNA packaged with TFAM and protamine. Gel shift analysis of pDNA packaged with TFAM (A) and protamine (B). pDNA was packaged with TFAM or protamine at various molar ratios (molar ratio = 0; lane 1 and 7, 1; lane 2 and 8, 50; lane 3 and 9, 100; lane 4 and 10, 500; lane 5 and 11, 1000; lane 6 and 12), and then the resulting products were subjected to agarose gel electrophoresis with pAsp (lanes 1–6) or without pAsp (lanes 7–12).

3.4. Evaluation of transcription efficiency of different structured DNA packaged with TFAM

To determine whether the transcriptional activation of DNA packaged with TFAM is influenced by the structure of DNA, we compared the transcription efficiency of a TFAM/DNA complex in the case of pDNA (circular structure, 6445 bp) and short linear DNA (linear structure, 1324 bp) preparations. Activation and inhibition of transcription were observed in the case of both pDNA and short linear DNA, but the optimal molar ratio for activating transcription was different (Figs. 3A, B, closed symbols). The transcription efficiency of pDNA was the highest when pDNA was packaged at a molar ratio of 375 (Fig. 3A, closed diamonds), while, for short linear DNA, the highest value was observed at a molar ratio of 75 (Fig. 3B, closed triangles). The highest transcription efficiency of the TFAM/pDNA complex was 1.8-fold greater than that for naked pDNA, while the value for short linear DNA was 1.3-fold. A previous report showed that super coiled DNA was activated to a greater extent by TFAM than relaxed circular DNA [28]. It seemed that the conformational change for transcription activation might be limited to linear DNA. In the case of protamine, the transcription of the DNA complex was greatly inhibited and no activation was found in the case of both pDNA and short linear DNA (Fig. 3A, B, open symbols).

Based on the data shown in Fig. 3A, B (closed symbols), we converted the molar ratios to the base-pair intervals required to TFAM to bind to DNA (bp intervals) on the X-axis (Fig. 3C, closed

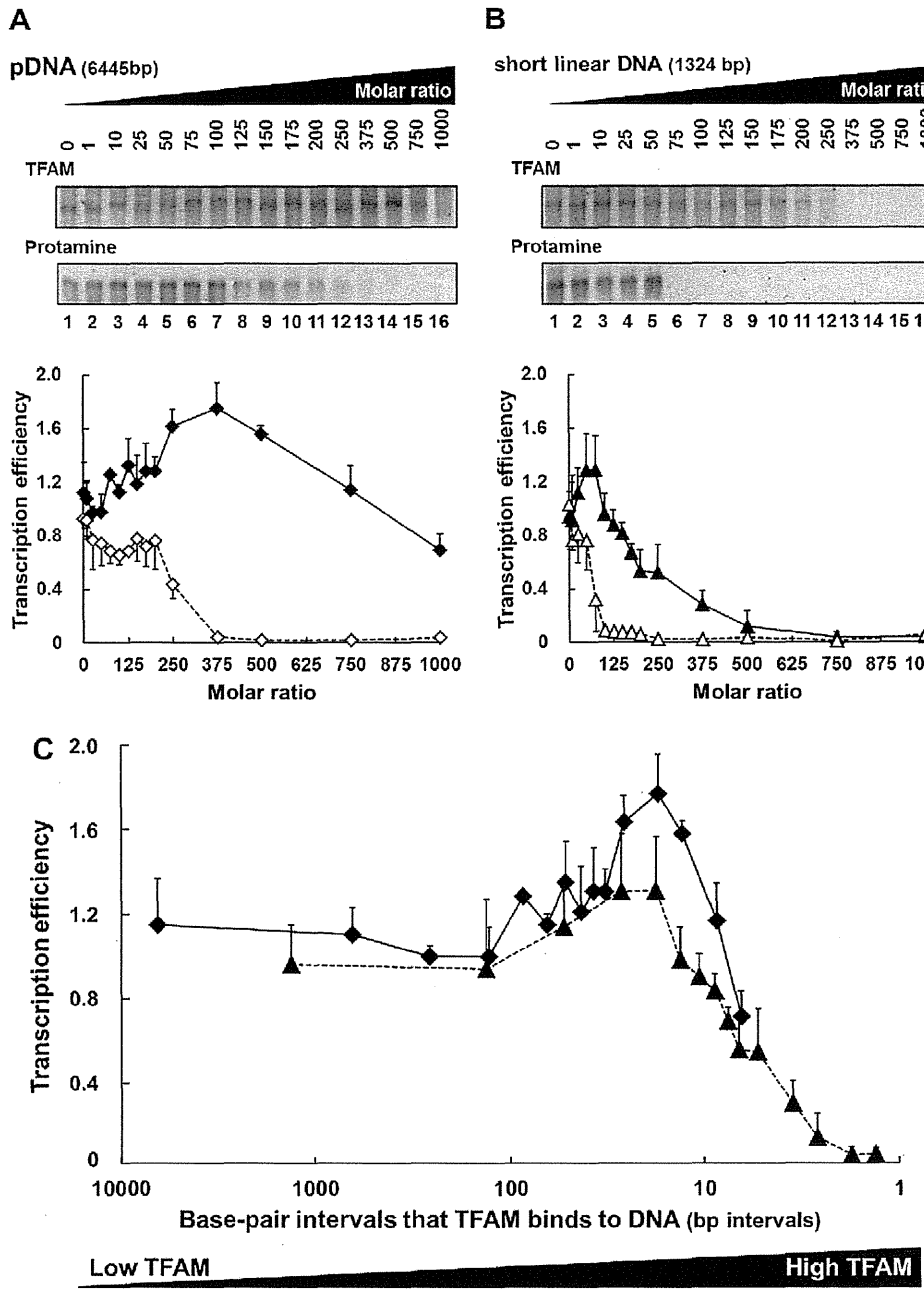

Fig. 3. In vitro transcription assay of DNA packaged with TFAM and protamine. pDNA (A, circular structure, 6445 bp) and short linear DNA (B, linear structure, 1324 bp) were packaged with TFAM and protamine at various molar ratios, and then subjected to an in vitro transcription assay. Electrophoresis gel data for transcripts after in vitro transcription reactions (upper part). Transcription efficiencies of DNA packaged with TFAM (closed symbols) and protamine (open symbols) were calculated based on the relative intensity of transcript band (lower part). Data are presented as the mean ± SD ($n = 3$). Based on the data shown in Fig. 3A, B (closed symbols), we converted the molar ratios to base-pair intervals that TFAM binds to DNA (bp intervals) in the X-axis (C). Closed diamonds and closed triangles indicate the values using pDNA and short linear DNA, respectively. Data are presented as the mean ± SD ($n = 3$).

diamonds, pDNA; closed triangles, short linear DNA).The base-pair intervals were calculated, when a DNA complex was formed at the optimal molar ratio for transcriptional activation (see Supplementary material for details).The values were calculated to be 17.1 and 17.6 in the case of pDNA and short linear DNA, respectively. These values are in general agreement with values previously reported by Kang and co-workers. They showed that one molecule of TFAM for every 20 bp activated transcription by in vitro transcription using mitochondrial RNA polymerase and mtDNA [21,28]. Based on this stoichiometric consideration, we speculated that transcription might be activated at the optimal DNA-conformation, when TFAM binds to DNA at the appropriate interval, as shown in Fig. 5A.

3.5. Investigation of transcription inhibition by excess TFAM using in vitro transcription assay

At high molar ratios, the transcription of DNA packaged with TFAM was inhibited (Fig. 3A, B). In such situation, a number of unbound TFAM molecules might interfere with the transcription reaction by T7 RNA polymerase. To validate this consideration, a

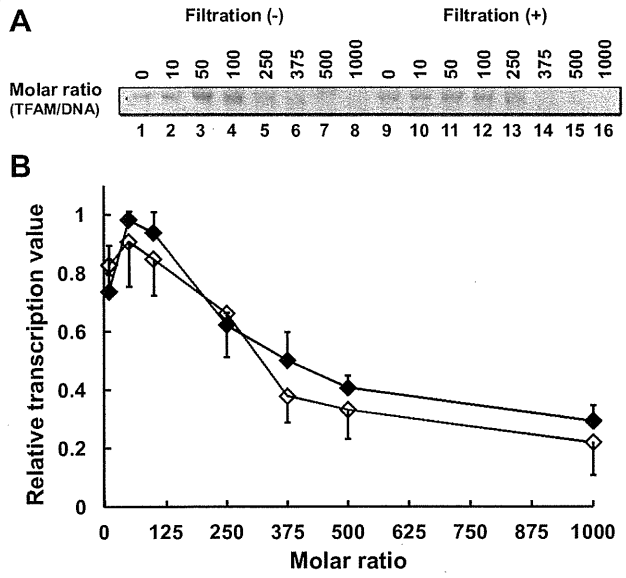

Fig. 4. In vitro transcription assay of a TFAM/pDNA complex before and after ultrafiltration. Electrophoresis gel data of transcripts after in vitro transcription reactions (A). pDNA were packaged with TFAM at various molar ratios (molar ratio = 0; lane 1 and 9, 10; lane 2 and 10, 50; lane 3 and 11, 100; lane 4 and 12, 250; lane 5 and 13, 375; lane 6 and 14, 500; lane 7 and 15, 1000; lane 8 and 16), and then subjected to in vitro transcription assay before ultrafiltration (lanes 1–8) and after ultrafiltration (lanes 9–16). Relative transcription value was calculated as follows (B), transcription efficiency of samples was normalized by maximum transfection efficiency among samples. Relative transcription values are indicated before (closed symbols) ultrafiltration and after (open symbols) ultrafiltration. Data are presented as the mean ± SD ($n = 3$).

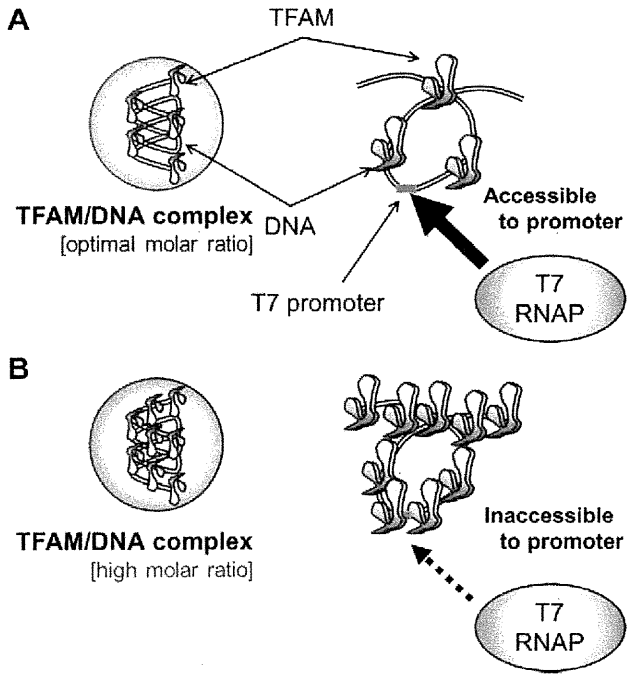

Fig. 5. Schematic illustration of DNA packaged with TFAM and the transcriptional manner. TFAM might form active DNA conformation for the transcription process, where DNA is bent or supercoiled for recruiting T7 RNA polymerase (T7 RNAP) (A). On the other hand, the overpackaging of DNA by excess TFAM would inhibit transcription, because T7 RNA polymerase might be inaccessible to the T7 promoter (B).

transcription assay using TFAM/pDNA complex was carried out after removing unbound TFAM by ultrafiltration. pDNA were packaged with TFAM at various molar ratios, and then subjected to in vitro transcription assay before and after ultrafiltration to remove unbound TFAM. Fig. 4A shows electrophoresis gel data of transcripts before ultrafiltration (Fig. 4A, lanes 1–8) and after ultrafiltration (Fig. 4A, lanes 9–16). Relative transcription value was normalized by maximum transfection efficiency among samples (Fig. 4B, closed diamonds, before filtration; open diamonds, after filtration).

If unbound TFAM interferes with the transcription reaction by T7 RNA polymerase, the transcription would be expected to be accelerated after the removal of unbound TFAM. However, the quantitative data showed that the transcription was inhibited to the same extent both before and after ultrafiltration (Fig. 4), indicating that transcriptional inhibition was not largely involved with the interference of transcription reaction by T7 RNA polymerase. This supports the view that the inhibition of transcription by TFAM is dependent on another factor, excess TFAM might bind to DNA and, as a result, decrease the recognition affinity of the T7 promoter by T7 RNA polymerase via the overpackaging of DNA (Fig. 5B).

4. Discussion

We first investigated the physicochemical properties of pDNA complexes when packaged with TFAM and protamine. In the case of protamine, negatively charged particles were converted into positively charged particles at a molar ratio of 500 (Fig. 1B, open diamonds). In this electrostatic inversion point, which is calculated to be a ± charge ratio of 2.4, excess protamine would contribute to the formation of positively charged particles. On the other hand, in the case of TFAM, the ζ potentials of the pDNA complexes were negatively charge at all molar ratios (Fig. 1B, closed diamonds). TFAM possesses high mobility group domains that contain both cationic and anionic amino residues [13,29]. Based on our results and this report, we conclude that the binding of cationic amino residues in TFAM to DNA is possible and, when this occurs, the anionic amino residues would be displayed on the surface of the TFAM/pDNA complex.

Electrophoretic mobility shift assay data showed that pDNA was efficiently released from a protamine/pDNA complex in the presence of pAsp (Fig. 2B, lanes 7–12), whereas pDNA release was not observed in the case of the TFAM/pDNA complex with pAsp treatment (Fig. 2A, lanes 7–12). It is presumed that pAsp might not be accessible to the TFAM/pDNA complex, because the TFAM/pDNA complex is negatively charged. In addition, EtBr was able to intercalate with the TFAM/pDNA complex, even at high molar ratios (Fig. 2A, lanes 5 and 6), although the protamine/pDNA complex was not detected under the same conditions (Fig. 2B, lanes 5 and 6). These results suggest that a TFAM/pDNA complex might be more loosely formed compared to a protamine/pDNA complex.

From the viewpoint of the unique structure of TFAM, we considered the reasons for why transcription is activated at specific conditions as shown in Fig. 3. One possibility is that TFAM might form a DNA conformation that is beneficial for activating transcription via non-specific binding, in which DNA would be easily recognized by T7 RNA polymerase, as shown in Fig. 5A. A recent crystallographic analysis of TFAM provides support for this possibility [29]. In the study, the crystal structure of full-length TFAM in complex with an oligonucleotide containing the LSP sequence was analyzed and the results suggest that TFAM causes the LSP to bend, thus creating an optimal DNA arrangement for transcriptional initiation. It was hypothesized that TFAM might play a role in the

structural change to strengthen the affinity of mitochondrial RNA polymerase for mtDNA, resulting in transcription activation.

Our findings indicated that DNA packaged with TFAM would have a great advantage over one packaged with protamine from the viewpoint of transcription efficiency. We also found that the TFAM could activate the transcription process with packaged DNA at the optimal molar ratio of DNA/TFAM. Moreover, a noteworthy point is that this study is the first trial to evaluate the effect of DNA packaged with TFAM on the transcription process using T7 RNA polymerase and DNA containing the T7 promoter. Collectively, our findings would largely contribute to the development of mitochondrial transgene methodology. In the future, we plan to investigate the function of DNA packaged with TFAM in mitochondria of living cells, using our mitochondrial matrix delivery system, a MITO-Porter that delivers cargoes into the mitochondrial matrix via membrane fusion [30–33]. Studies in this area are currently underway.

Acknowledgements

This work was supported, in part by, a Grant-in-Aid for Young Scientists (A) and a Grant-in-Aid for Scientific Research (S) from the Ministry of Education, Culture, Sports, Science and Technology of Japanese Government (MEXT), the Program for Promotion of Fundamental Studies in Health Sciences of the National Institute of Biomedical Innovation, Japan (NIBIO). We thank Dr. Milton Feather for his helpful advice in writing the manuscript.

Appendix A. Supplementary material

Supplementary material associated with this article can be found, in the online version, at http://dx.doi.org/10.1016/j.fob.2012.06.001.

References

[1] Wallace, D.C. (2005) A mitochondrial paradigm of metabolic and degenerative diseases, aging, and cancer: a dawn for evolutionary medicine. Annu. Rev. Genet. 39, 359–407.
[2] Suzuki, T. and Nagao, A. (2011) Human mitochondrial tRNAs: biogenesis, function, structural aspects, and diseases. Annu. Rev. Genet. 45, 299–329.
[3] Pichon, C., Billiet, L. and Midoux, P. (2010) Chemical vectors for gene delivery: uptake and intracellular trafficking. Curr. Opin. Biotechnol. 21, 640–645.
[4] Matsumoto, Y., Itaka, K., Yamasoba, T. and Kataoka, K. (2009) Intranuclear fluorescence resonance energy transfer analysis of plasmid DNA decondensation from nonviral gene carriers. J. Gene Med. 11, 615–623.
[5] Yamada, Y., Nomura, T., Harashima, H., Yamashita, A. and Yui, N. (2012) Post-nuclear gene delivery events for transgene expression by biocleavable polyrotaxanes. Biomaterials 33, 3952–3958.
[6] Li, S., Rizzo, M.A., Bhattacharya, S. and Huang, L. (1998) Characterization of cationic lipid–protamine–DNA (LPD) complexes for intravenous gene delivery. Gene Ther. 5, 930–937.
[7] Warrant, R.W. and Kim, S.H. (1978) Alpha-helix-double helix interaction shown in the structure of a protamine-transfer RNA complex and a nucleoprotamine model. Nature 271, 130–135.
[8] Kanki, T., Nakayama, H., Sasaki, N., Takio, K., Alam, T.I., Hamasaki, N. and Kang, D. (2004) Mitochondrial nucleoid and transcription factor A. Ann. N. Y. Acad. Sci. 1011, 61–68.
[9] Iborra, F.J., Kimura, H. and Cook, P.R. (2004) The functional organization of mitochondrial genomes in human cells. BMC Biol. 2, 9.
[10] Bogenhagen, D.F., Rousseau, D. and Burke, S. (2008) The layered structure of human mitochondrial DNA nucleoids. J. Biol. Chem. 283, 3665–3675.
[11] Gilkerson, R.W. (2009) Mitochondrial DNA nucleoids determine mitochondrial genetics and dysfunction. Int. J. Biochem. Cell Biol. 41, 1899–1906.
[12] Holt, I.J., He, J., Mao, C.C., Boyd-Kirkup, J.D., Martinsson, P., Sembongi, H., Reyes, A. and Spelbrink, J.N. (2007) Mammalian mitochondrial nucleoids: organizing an independently minded genome. Mitochondrion 7, 311–321.
[13] Gangelhoff, T.A., Mungalachetty, P.S., Nix, J.C. and Churchill, M.E. (2009) Structural analysis and DNA binding of the HMG domains of the human mitochondrial transcription factor A. Nucleic Acids Res. 37, 3153–3164.
[14] Fisher, R.P. and Clayton, D.A. (1988) Purification and characterization of human mitochondrial transcription factor 1. Mol. Cell. Biol. 8, 3496–3509.
[15] Dairaghi, D.J., Shadel, G.S. and Clayton, D.A. (1995) Addition of a 29 residue carboxyl-terminal tail converts a simple HMG box-containing protein into a transcriptional activator. J. Mol. Biol. 249, 11–28.
[16] Fisher, R.P., Lisowsky, T., Parisi, M.A. and Clayton, D.A. (1992) DNA wrapping and bending by a mitochondrial high mobility group-like transcriptional activator protein. J. Biol. Chem. 267, 3358–3367.
[17] Scarpulla, R.C. (2008) Transcriptional paradigms in mammalian mitochondrial biogenesis and function. Physiol. Rev. 88, 611–638.
[18] Kang, D., Kim, S.H. and Hamasaki, N. (2007) Mitochondrial transcription factor A (TFAM): roles in maintenance of mtDNA and cellular functions. Mitochondrion 7, 39–44.
[19] Pohjoismaki, J.L., Wanrooij, S., Hyvarinen, A.K., Goffart, S., Holt, I.J., Spelbrink, J.N. and Jacobs, H.T. (2006) Alterations to the expression level of mitochondrial transcription factor A, TFAM, modify the mode of mitochondrial DNA replication in cultured human cells. Nucleic Acids Res. 34, 5815–5828.
[20] Kaufman, B.A., Durisic, N., Mativetsky, J.M., Costantino, S., Hancock, M.A., Grutter, P. and Shoubridge, E.A. (2007) The mitochondrial transcription factor TFAM coordinates the assembly of multiple DNA molecules into nucleoid-like structures. Mol. Biol. Cell 18, 3225–3236.
[21] Kukat, C., Wurm, C.A., Spahr, H., Falkenberg, M., Larsson, N.G. and Jakobs, S. (2011) Super-resolution microscopy reveals that mammalian mitochondrial nucleoids have a uniform size and frequently contain a single copy of mtDNA. Proc. Natl. Acad. Sci. U S A 108, 13534–13539.
[22] Matsushima, Y., Goto, Y. and Kaguni, L.S. (2010) Mitochondrial Lon protease regulates mitochondrial DNA copy number and transcription by selective degradation of mitochondrial transcription factor A (TFAM). Proc. Natl. Acad. Sci. U S A 107, 18410–18415.
[23] Seidel-Rogol, B.L. and Shadel, G.S. (2002) Modulation of mitochondrial transcription in response to mtDNA depletion and repletion in HeLa cells. Nucleic Acids Res. 30, 1929–1934.
[24] Nayak, D., Guo, Q. and Sousa, R. (2009) A promoter recognition mechanism common to yeast mitochondrial and phage t7 RNA polymerases. J. Biol. Chem. 284, 13641–13647.
[25] Shutt, T.E. and Gray, M.W. (2006) Bacteriophage origins of mitochondrial replication and transcription proteins. Trends Genet. 22, 90–95.
[26] Claros, M.G. and Vincens, P. (1996) Computational method to predict mitochondrially imported proteins and their targeting sequences. Eur. J. Biochem. 241, 779–786.
[27] Sorgi, F.L., Bhattacharya, S. and Huang, L. (1997) Protamine sulfate enhances lipid-mediated gene transfer. Gene Ther. 4, 961–968.
[28] Fukuoh, A., Ohgaki, K., Hatae, H., Kuraoka, I., Aoki, Y., Uchiumi, T., Jacobs, H.T. and Kang, D. (2009) DNA conformation-dependent activities of human mitochondrial RNA polymerase. Genes Cells 14, 1029–1042.
[29] Rubio-Cosials, A. et al. (2011) Human mitochondrial transcription factor A induces a U-turn structure in the light strand promoter. Nat. Struct. Mol. Biol. 18, 1281–1289.
[30] Yasuzaki, Y., Yamada, Y. and Harashima, H. (2010) Mitochondrial matrix delivery using MITO-Porter, a liposome-based carrier that specifies fusion with mitochondrial membranes. Biochem. Biophys. Res. Commun. 397, 181–186.
[31] Yamada, Y. et al. (2008) MITO-Porter: a liposome-based carrier system for delivery of macromolecules into mitochondria via membrane fusion. Biochim. Biophys. Acta 1778, 423–432.
[32] Yamada, Y., Furukawa, R., Yasuzaki, Y. and Harashima, H. (2011) Dual function MITO-porter, a nano carrier integrating both efficient cytoplasmic delivery and mitochondrial macromolecule delivery. Mol. Ther. 19, 1449–1456.
[33] Yamada, Y. and Harashima, H. (2012) Delivery of bioactive molecules to the mitochondrial genome using a membrane-fusing, liposome-based carrier, DF-MITO-Porter. Biomaterials 33, 1589–1595.

SUPPLEMENTARY MATERIAL

1 The properties of prepared TFAM

In this experiment, human TFAM protein with N-terminal His tag was expressed in bacterial cells, purified by nickel-nitrilotriacetic acid chromatography, and finally dialyzed. The purified protein (theoretical molecular weight, approximately 27 kDa) was analyzed by SDS-PAGE as shown in Figure S1. As a result, we observed the bands correspond to recombinant human TFAM, when nickel-nitrilotriacetic acid chromatography (lane 7) and dialysis (lane 8) were performed.

Figure S1. SDS-PAGE analysis of prepared of human TFAM

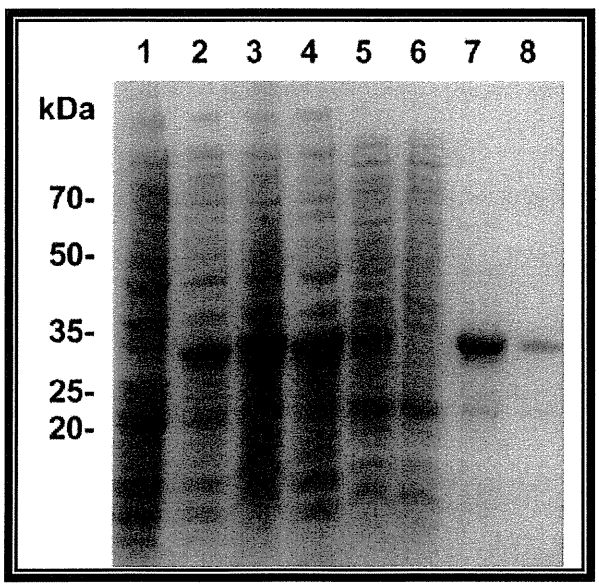

1: non-induced cell; 2: induced cell; 3: crude cell lysate; 4: insoluble fraction; 5 soluble fraction; 6: Ni-column flow-through; 7: eluate; 8: dialyzed protein.

2 Estimation of the base-pair intervals required for TFAM to bind to DNA for transcription activation

Based on the data shown in Figures 3A, 3B (closed symbols), we converted the molar ratios to the base-pair intervals required for TFAM to bind to DNA (bp intervals) on the X-axis (Figure 3C) using Equation S1.

Equation S1

Base-pair intervals required for TFAM to bind to DNA (bp intervals)

= base-pair number of DNA [A] / value for molar ratio of TFAM/DNA [B]

Note that molar ratio of TFAM/DNA indicates the number of TFAM molecules per DNA molecule.

The transcription efficiency of pDNA was the highest when pDNA (6445 bp) was packaged at a molar ratio of 375 (Figure 3A), while the highest value for short linear DNA (1324 bp) was observed at a molar ratio of 75 (Figure 3B). We calculated the base-pair number of DNA per TFAM molecule when a DNA complex was formed at the optimal molar ratio for the transcription activation using Equation S1.

Example calculation,

Base-pair intervals required for TFAM to bind to DNA (bp intervals), to form a DNA complex with pDNA (6445 bp) at a molar ratio of 375

= base-pair number of DNA [A] / value for molar ratio of TFAM/DNA [B]

= 6445 [A] / 375 [B] = 17.1

In the same procedure,

The base-pair intervals required for TFAM to bind to DNA (bp intervals), to form a DNA complex with short linear DNA (1324 bp) at a molar ratio of 75

are calculated to be 17.6.

International Journal of Cardiology 162 (2013) 234–239

Contents lists available at ScienceDirect

International Journal of Cardiology

journal homepage: www.elsevier.com/locate/ijcard

Association between cardiopulmonary exercise and dobutamine stress testing in ambulatory patients with idiopathic dilated cardiomyopathy: A comparison with peak VO_2 and VE/VCO_2 slope

Takahiro Okumura [a], Akihiro Hirashiki [a,*], Sumio Yamada [b], Hidehito Funahashi [a], Satoru Ohshima [a], Yuji Kono [c], Xian Wu Cheng [a], Kyosuke Takeshita [a], Toyoaki Murohara [a]

[a] Department of Cardiology, Nagoya University Graduate School of Medicine, Nagoya, Japan
[b] School of Health Sciences, Nagoya University, Nagoya, Japan
[c] Program in Physical and Occupational Therapy, Nagoya University Graduate School of Medicine, Nagoya, Japan

ARTICLE INFO

Article history:
Received 31 October 2010
Received in revised form 18 February 2011
Accepted 13 May 2011

Keywords:
Cardiomyopathy
Dobutamine
Cardiopulmonary exercise testing

ABSTRACT

Background: Both peak VO_2 and VE/VCO_2 slope are considered to be useful predictors of cardiovascular events. The left ventricular (LV) response to dobutamine stress testing (DST) also provides useful prognostic information. However, the relationship between these variables has not been fully investigated. Therefore, the aim of this study is to investigate the association between myocardial contractile reserve measured by DST and cardiopulmonary exercise testing (CPX) variables in patients with idiopathic dilated cardiomyopathy (IDCM).

Methods: Thirty-eight patients were subjected to CPX as well as cardiac catheterization for measurement of LV pressure. The maximum first derivative of LV pressure (LV dP/dt_{max}) was measured at baseline and during dobutamine infusion at incremental doses of 5, 10, and 15 $\mu g\ kg^{-1}\ min^{-1}$. LV dP/dt_{max} at baseline and the percentage increase in LV dP/dt_{max} (ΔLV dP/dt_{max}) induced by DST served as indices of LV contractility and myocardial contractile reserve, respectively.

Results: Peak VO_2, and VE/VCO_2 slope were 18.6 mL kg^{-1} min^{-1} and 32.3, respectively. Peak VO_2 was not correlated with LV dP/dt_{max} at baseline. However, peak VO_2 was significantly correlated with ΔLV dP/dt_{max}, and the correlation became more pronounced as the dose of dobutamine was increased. There was no correlation between VE/VCO_2 slope and ΔLV dP/dt_{max}. Multivariate regression analysis revealed that ΔLV dP/dt_{max} was independently correlated with peak VO_2 ($p=0.011$).

Conclusions: Peak VO_2, but not VE/VCO_2 slope, may reflect myocardial contractile reserve in ambulatory patients with IDCM. This study population is small, and therefore large confirmatory studies are needed.

1. Introduction

Heart failure (HF), a major and growing public health problem, appears to result not only from cardiac overload or injury but also from a complex interplay among genetic, neurohormonal, and biochemical changes acting on cardiac myocytes, the cardiac interstitium, or both [1]. Exercise tolerance reflects a number of prognostically important factors, including cardiac function, oxygen-carrying capacity, and autonomic nervous system balance [2–4]. Cardiopulmonary exercise testing (CPX) is a diagnostic tool used to detect serial changes in exercise capacity, and it is of particular benefit for patients with chronic HF to assess peak oxygen uptake (peak VO_2) and minute ventilation/carbon dioxide production (VE/VCO_2) slope since those parameters have functioned as predictors for overall mortality or determinants of risk stratification for such individuals [5–9].

Peak VO_2 seems to be accurate for evaluating the functional status of patients with chronic HF and non-ischemic dilated cardiomyopathy because the changes in echocardiographic variables assessed by dobutamine echocardiography are well correlated with peak VO_2 [10–13]. Meanwhile, the mechanisms of a high VE/VCO_2 slope are multifactorial. Abnormalities of ventilator reflex control, pulmonary hemodynamics and low cardiac index during exercise are all possible correlations [14,15], however, its direct association with inotropic effect on cardiac hemodynamics has remained unclear.

Therefore, this study aimed to investigate a potential association between CPX variables and the left ventricular (LV) responses during dobutamine stress testing (DST) in ambulatory patients with idiopathic dilated cardiomyopathy (IDCM).

* Corresponding author at: Department of Cardiology, Nagoya University Graduate School of Medicine, 65 Tsurumai-cho, Shouwa-ku, Nagoya 466-8560, Japan. Tel.: +81 52 744 2147; fax: +81 52 744 2211.
E-mail address: hirasiki@med.nagoya-u.ac.jp (A. Hirashiki).

0167-5273/$ – see front matter © 2011 Elsevier Ireland Ltd. All rights reserved.
doi:10.1016/j.ijcard.2011.05.065

2. Methods

2.1. Patients

We studied 38 consecutive IDCM patients at Nagoya University Hospital between December 2007 and December 2009. All patients were in sinus rhythm and on optimal pharmacological therapy, according to current guidelines for treatment of HF [16]. Ongoing medical therapy was kept unchanged at the time of the stress test. No patients had implantable cardioverter-defibrillators or pacemakers. Each patient was hospitalized for examination and underwent laboratory measurements, a pulmonary functional test, echocardiography, CPX, and cardiac catheterization. IDCM was defined on the basis of the presence of both a reduced LV ejection fraction (LVEF) (<50% as determined by contrast left ventriculography) and a dilated LV cavity, in the absence of coronary or valvular heart disease, hypertension, or secondary cardiac muscle disease caused by any known systemic condition, as determined by endomyocardial biopsy [17]. The study protocol was approved by the Ethics Review Board of Nagoya University School of Medicine (approval no. 359), and written informed consent was obtained from all study subjects. Blood samples were collected from the antecubital vein of fasted patients after they had rested for 20 min in the supine position. Routine blood biochemical analysis was performed in addition to measurement of the plasma brain natriuretic peptide (BNP), renin activity, aldosterone, epinephrine, and norepinephrine. The estimated glomerular filtration rate (GFR) was calculated by using an equation modified for Japanese: estimated GFR ($mL\,min^{-1}$) = 194 × (serum creatinine) $^{-1.094}$ × (age in years) $^{-0.287}$. To adjust for female sex, the equation was: estimated GFR female = estimated GFR × 0.739 [18].

2.2. Echocardiography

Standard M-mode and two-dimensional echocardiography, Doppler blood flow, and tissue Doppler imaging measurements were performed in agreement with the American Society of Echocardiography guidelines using the Vivid 7 system (Vivid 7, GE Healthcare, Milwaukee, WI, USA) [19]. Septal and posterior LV wall thicknesses were obtained from the parasternal long-axis view. The LV end-diastolic and end-systolic volumes were obtained from 4 apical and 2 chamber views [20]. The LVEF was calculated from 2-dimensional apical images according to the formula of modified Simpson's method. Pulse-wave Doppler echocardiography was used to assess mitral peak early (E) and late wave flow velocity and E-wave deceleration time. The tissue Doppler imaging wave sample of the mitral annulus was obtained from the septal side of the apical 4-chamber view. Analysis was performed for the early (Ea) diastolic peak velocity. The ratio of early transmitral flow velocity to early diastolic mitral annular velocity (E/Ea) was taken as an estimate of LV filling pressure [21].

2.3. CPX procedure and data collection

Each patient underwent CPX at a progressively increasing work rate to maximum tolerance on a cycle ergometer. The test protocol was in accordance with the recommendations of the American Thoracic Society and American College of Chest Physicians [22]. The oxygen and carbon dioxide sensors were calibrated before each test using gasses with known oxygen, nitrogen, and carbon dioxide concentrations. The flow sensor was also calibrated before each test using a 3-L syringe. All patients started at 10 W for 3 min warm-up, followed by a 10 W/min ramp increment protocol up to the termination criteria. Test termination criteria consisted of patient request, volitional fatigue, ventricular tachycardia, ≥2 mm of horizontal or downsloping ST segment depression, or a drop in systolic blood pressure ≥20 mm Hg during exercise. A qualified exercise physiologist conducted each test with physician supervision. A 12-lead electrocardiogram was monitored continuously, and blood pressure was measured every minute during exercise and throughout the recovery period. Respiratory gas exchange variables, including VO_2, VCO_2, and VE, were acquired continuously throughout the exercise testing using an Ergospirometry Oxycon Pro (Care Fusion; Sun Diego, CA, USA), and the gas-exchange data were obtained breath-by-breath. Peak VO_2 was expressed as the highest 30-second average value obtained during the last stage of the exercise test, and the peak respiratory exchange ratio was the highest 30-second averaged value during the last stage of the test. The VE/VCO_2 slope was determined by using linear regression analysis of VE and VCO_2 obtained during exercise [23]. The ventilatory threshold was determined in all patients by the classical method [24,25].

2.4. Cardiac catheterization and DST

All patients initially underwent routine diagnostic left and right heart catheterization. A 6-F fluid-filled pigtail catheter with a high-fidelity micromanometer (CA-61000-PLB Pressure-tip Catheter, CD Leycom, Zoetermeer, The Netherlands) was placed in the LV cavity for measurement of LV pressure. We evaluated the maximum first derivative of LV pressure (LV dP/dt_{max}) as an index of LV contractility, as previously described [26]. After collection of baseline hemodynamic data, dobutamine was infused intravenously at incremental doses of 5, 10, and 15 $\mu g\,kg^{-1}\,min^{-1}$, and hemodynamic measurements were made at the end of each 5-minute infusion period. In addition, we calculated ΔLV dP/dt_{max} as an index of myocardial contractile reserve [27]. ΔLV dP/dt_{max} was defined as the percentage increase in LV dP/dt_{max} induced by dobutamine, and this index was defined on the basis of the formula ΔLV dP/dt_{max} (x) (%) = [LV dP/dt_{max} (x) − LV dP/dt_{max} (baseline)] / LV dP/dt_{max} (baseline), where x = the dose of dobutamine ($\mu g\,kg^{-1}\,min^{-1}$).

2.5. Statistical analysis

Data are presented as means ± standard deviation. All statistical analyses were performed with the SPSS 17.0 software package (SPSS Inc., Chicago, IL, USA). To investigate the association between myocardial contractile reserve measured by DST and CPX variables, the relationship between echocardiographic index, hemodynamic parameters or biomarkers, and CPX variables was analyzed by using correlation coefficients and a linear regression analysis. As for the differences of measurements between two groups, normally distributed variables were compared by the Student's t test and non-normally distributed variables by the Mann–Whitney U test. Differences between three groups were analyzed by a two-way ANOVA followed by Turkey's post hoc test. Four major factors used widely in clinical practice — the plasma BNP level (biomarker), E/Ea ratio (LV diastolic performance), LVEF (LV systolic performance), and ΔLV dP/dt_{max} (10) — were used in a multivariate regression analysis to determine independent factors of peak VO_2 and VE/VCO_2 slope. A p-value of <0.05 was considered statistically significant.

3. Results

3.1. Baseline clinical characteristics

Baseline clinical characteristics of the patients are shown in Table 1. The mean age was 51.3 years old, and 92% of patients had mild symptoms, classified as New York Heart Association functional class I or II. Twenty-one (55%) patients had been treated with β-blockers. No patients had abnormal respiratory function. The peak VO_2 was 18.6 ± 5.2 $mL\,kg^{-1}\,min^{-1}$ and the VE/VCO_2 slope was 32.3 ± 10.8. The heart rate at baseline and peak exercise was 85.9 ± 16.1 and 131.1 ± 22.4 bpm, respectively. The mean LVEF measured by left ventriculography was 32.5%. There were no patients with severe pulmonary hypertension.

3.2. Hemodynamic responses by DST

Hemodynamic responses to intravenous dobutamine infusion are shown in Table 2. No complications occurred in any of the study subjects during the dobutamine stress protocol. The heart rate, LV systolic pressure and LV dP/dt_{max} were increased as the dose of dobutamine was increased. Contractile response (ΔLV dP/dt_{max}) increased significantly as the dose of dobutamine was increased (Fig. 1). There were no significant differences in LV dP/dt_{max} (5), LV dP/dt_{max} (10) between treatment groups with or without ß-blocker, whereas LV dP/dt_{max} (15) was only significantly lower in the ß-blocker (+) group than in the ß-blocker (−) group (Table 3). We observed that there were also no significant differences in all ΔLV dP/dt_{max} between two groups, even though it was increased as the dose of dobutamine was increased.

3.3. Myocardial contractile reserve and CPX parameters

The correlations between patient characteristics, biomarkers, echocardiographic data, or hemodynamic parameters and peak VO_2 or VE/VCO_2 slope are shown in Table 4. The plasma BNP level and E/Ea ratio were significantly correlated with peak VO_2 ($r = -0.538$, $r = -0.390$, respectively). The plasma BNP level was also correlated with VE/VCO_2 slope ($r = 0.764$). However, LVEF was not significantly correlated with peak VO_2 and VE/VCO_2 slope. Whereas the LV dP/dt_{max} at baseline was not significantly correlated with peak VO_2 ($r = 0.286$, $p = 0.081$), the LV dP/dt_{max} under the dobutamine infusion was significantly correlated with peak VO_2 (LV dP/dt_{max} (5); $r = 0.339$, LV dP/dt_{max} (10); $r = 0.428$, LV dP/dt_{max} (15); $r = 0.490$, respectively). In addition, the ΔLV dP/dt_{max} was significantly correlated with peak VO_2, and the correlation became more pronounced as the dose of dobutamine was increased (ΔLV dP/dt_{max} (5); $r = 0.329$, ΔLV dP/dt_{max} (10); $r = 0.508$, ΔLV dP/dt_{max} (15); $r = 0.601$, respectively) (Fig. 2). In contrast, no significant correlation between ΔLV dP/dt_{max} and

Table 1
Baseline clinical characteristics (n = 38).

Age (yrs)	51.3 ± 13.1
Gender, male/female	25/13
Body mass index (kg m^{-2})	23.5 ± 4.4
NYHA functional class (I/II/III/IV)	(23/12/3/0)
Medication, n (%)	
β-blockers	21 (55)
ACE inhibitors	6 (16)
ARBs	
19 (50)	
Diuretics	21 (55)
Spironoractone	17 (43)
Statins	
5 (13)	
Laboratory measurements	
Hemoglobin (g dL^{-1})	13.5 ± 1.6
Estimated GFR (mL min^{-1})	68.4 ± 28.3
Plasma norepinephrine (ng mL^{-1})	0.569 ± 0.311
Plasma BNP (pg mL^{-1})	203.1 ± 225.5
Respiratory function	
FVC% predicted	104.0 ± 15.0
FEV1% predicted	79.3 ± 6.8
DL_{CO} (mL min^{-1} mm Hg^{-1})	20.7 ± 6.6
Echocardiography	
LV end-diastolic diameter (mm)	63.6 ± 9.2
LV end-systolic diameter (mm)	53.5 ± 10.7
Left atrial diameter (mm)	40.9 ± 8.5
E/A ratio	1.3 ± 0.8
Deceleration time (ms)	203.8 ± 60.8
E/Ea ratio	15.4 ± 8.8
MR (none or trivial/mild/moderate/severe)	(22/10/3/3)
CPX variables	
Baseline heart rate (beats min^{-1})	85.9 ± 16.1
Peak heart rate (beats min^{-1})	131.1 ± 22.4
Baseline systolic blood pressure (mm Hg)	118.4 ± 23.9
Peak systolic blood pressure (mm Hg)	159.3 ± 45.2
Peak VO_2 (mL kg^{-1} min^{-1})	18.6 ± 5.2
VE/VCO_2 slope	32.3 ± 10.8
$\Delta VO_2/\Delta WR$ (mL min^{-1} W^{-1})	9.1 ± 2.9
Peak RER	1.08 ± 0.09
Cardiac catheterization	
LV ejection fraction (%)	32.5 ± 10.4
LV end-diastolic volume (mL)	254.3 ± 92.7
LV end-systolic volume (mL)	183.2 ± 87.4
PAWP (mm Hg)	11.8 ± 5.8
Systolic PA pressure (mm Hg)	25.9 ± 9.3
Cardiac index (L min^{-1} m^{-2})	2.78 ± 0.52
LV end-diastolic pressure (mm Hg)	15.2 ± 8.7

Data are means ± SD.
NYHA = New York Heart Association; ACE = angiotensin-converting enzyme; ARB = angiotensin II receptor blocker; GFR = glomerular filtration rate; BNP = brain natriuretic peptide; FVC = forced vital capacity; FEV1% = forced expiratory volume in 1 second as percent of FVC; DLco = diffusing capacity for carbon monoxide; LV = left ventricular; E/Ea ratio = ratio of early transmitral flow velocity to early diastolic mitral annular velocity; MR = mitral regurgitation; CPX = cardiopulmonary exercise testing; peak VO_2 = peak oxygen uptake; VE/VCO_2 slope = the minute ventilation/carbon dioxide production; $\Delta VO_2/\Delta WR$ = the ratio of the increase in VO_2 to the increase in work rate; RER = respiratory exchange ratio; PAWP = pulmonary arterial wedge pressure; PA = pulmonary artery.

VE/VCO_2 slope was observed (ΔLV dP/dt_{max} (5); p = 0.257, ΔLV dP/dt_{max} (10); p = 0.161, ΔLV dP/dt_{max} (15); p = 0.085, respectively). Multivariate regression analysis revealed that ΔLV dP/dt_{max} (10) and plasma BNP level were independently correlated with peak VO_2 (p = 0.011, p = 0.001, respectively) (Table 5). We observed that plasma BNP levels was only independently significant correlated with VE/VCO_2 slope, whereas ΔLV dP/dt_{max} (10) was not significantly correlated with VE/VCO_2 slope (p = 0.708).

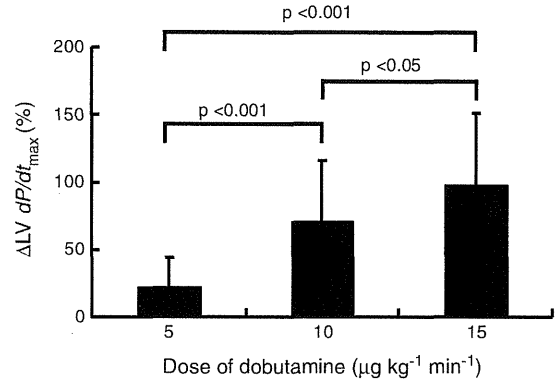

Fig. 1. Contractile response to dobutamine stress testing. Left ventricular hemodynamic response of 38 patients to dobutamine stress testing. Data are shown as means ± SD. ΔLV dP/dt_{max} increased significantly as the dose of dobutamine was increased.

4. Discussion

In the present study, we investigated the association between LV response to dobutamine and CPX variables to examine our hypothesis that myocardial contractile reserve correlates closely with exercise functional capacity. Our results showed that the myocardial contractile reserve measured by DST was strongly correlated with peak VO_2 as the dose of dobutamine was increased, whereas it was not correlated with VE/VCO_2 slope. In addition, the contractile reserve by DST was independently correlated with peak VO_2. These findings suggest that only peak VO_2, and not VE/VCO_2 slope, reflects myocardial contractile reserve in patients with IDCM. To our knowledge, this investigation is the first to report the relationship between myocardial contractile reserve as assessed by DST using directly measured LV pressure and CPX variables — especially the 2 major prognostic parameters, peak VO_2 and VE/VCO_2 slope — in patients with IDCM.

Peak VO_2 and VE/VCO_2 slope are 2 major powerful predictors of mortality in HF patients with severe systolic LV dysfunction [9], but a dissociation between peak VO_2 and VE/VCO_2 slope is occasionally seen in patients with HF. Peak VO_2, measured at the end of the test, is widely used as the diagnostic and prognostic surrogate marker in patients with HF [8]. However, the end point of an exercise test is greatly influenced by motivation on the part of the patients and the testing personnel [28]. In addition, cardiac output cannot be accurately estimated from CPX, largely because VO_2 is influenced by numerous central and peripheral factors [29]. On the other hand, a growing body of studies over last decade has demonstrated that VE/VCO_2 slope more powerfully predicts mortality or hospitalization than peak VO_2 among HF patients [30]. VE/VCO_2 slope is influenced not only cardiac function but also respiratory physiological deregulation such as ergoreflex or chemoreflex sensitivity, and inversely correlated with exercise tolerance in chronic HF [28].

Table 2
Hemodynamic response to intravenous dobutamine infusion.

Parameter	Baseline	Dobutamine (5 μg kg^{-1} min^{-1})	Dobutamine (10 μg kg^{-1} min^{-1})	Dobutamine (15 μg kg^{-1} min^{-1})
Heart rate (beats min^{-1})	74.0 ± 14.5	77.0 ± 16.3	88.8 ± 20.9	101.1 ± 23.8
LVSP (mm Hg)	122.0 ± 25.8	127.7 ± 31.4	139.5 ± 42.2	136.7 ± 35.4
LV dP/dt_{max} (mm Hg s^{-1})	1079.8 ± 299.4	1353.3 ± 583.8	1920.2 ± 891.3	2203.8 ± 994.1

Data are means ± SD.
LVSP = left ventricular systolic pressure; LV dP/dt_{max} = maximal first derivative of left ventricular pressure.

Table 3
Comparison of hemodynamic response by DST between treatment groups with or without ß-blocker.

Parameter	ß-blocker (−)(n = 17)	ß-blocker (+)(n = 21)	p-value
Heart rate (beats min^{-1})			
Baseline	79.5 ± 15.1	69.5 ± 12.8	0.04
Dobutamine (5 μg kg^{-1} min^{-1})	85.8 ± 13.9	69.9 ± 14.8	0.002
Dobutamine (10 μg kg^{-1} min^{-1})	103.3 ± 17.0	77.3 ± 16.1	0.00004
Dobutamine (15 μg kg^{-1} min^{-1})	118.6 ± 16.6	86.4 ± 18.5	0.000006
LVSP (mm Hg)			
Baseline	123.0 ± 27.0	121.1 ± 25.5	0.83
Dobutamine (5 μg kg^{-1} min^{-1})	130.1 ± 34.0	125.7 ± 29.9	0.68
Dobutamine (10 μg kg^{-1} min^{-1})	133.9 ± 33.2	144.0 ± 48.6	0.48
Dobutamine (15 μg kg^{-1} min^{-1})	132.7 ± 31.6	140.1 ± 38.8	0.55
LV dP/dt_{max} (mm Hg s^{-1})			
Baseline	159.2 ± 278.0	1019.3 ± 307.5	0.16
Dobutamine (5 μg kg^{-1} min^{-1})	1448.9 ± 624.8	1189.8 ± 357.1	0.13
Dobutamine (10 μg kg^{-1} min^{-1})	2073.3 ± 806.6	1646.6 ± 597.2	0.08
Dobutamine (15 μg kg^{-1} min^{-1})	2452.9 ± 1056.0	1851.5 ± 575.3	0.04
ΔLV dP/dt_{max}			
Dobutamine (5 μg kg^{-1} min^{-1})	26.2 ± 34.8	14.5 ± 9.4	0.16
Dobutamine (10 μg kg^{-1} min^{-1})	79.1 ± 45.2	56.4 ± 24.5	0.06
Dobutamine (15 μg kg^{-1} min^{-1})	110.1 ± 58.2	82.5 ± 34.5	0.09

Data are means ± SD.
DST = dobutamine stress testing; LVSP = left ventricular systolic pressure; LV dP/dt_{max} = maximal first derivative of left ventricular pressure; ΔLV dP/dt_{max} = the percentage increase in LV dP/dt_{max} induced by dobutamine.

Table 4
Correlation between ecocardiographic index, hymodynamic parameters or biomarkers and CPX variables.

	Peak VO_2		VE/VCO_2 slope	
	r	p-value	r	p-value
Age	0.076	0.651	0.070	0.677
Body mass index	−0.059	0.726	−0.439	0.006
Laboratory measurement				
Hemoglobin	0.203	0.222	−0.396	0.014
Estimated GFR	0.109	0.515	−0.112	0.504
Norepinephrine	−0.094	0.576	−0.230	0.165
Plasma BNP	−0.538	<0.001	0.764	<0.001
Echocardiography				
LV end-diastolic diameter	−0.306	0.062	0.268	0.104
LV end-systolic diameter	−0.297	0.070	0.332	0.042
Left atrial diameter	−0.314	0.055	0.332	0.041
E/A ratio	−0.275	0.094	0.750	<0.001
Decerelation time	0.114	0.496	−0.218	0.188
E/Ea ratio	−0.390	0.016	0.255	0.122
CPX variables				
Baseline heart rate	0.079	0.637	−0.291	0.0762
Peak heart rate	0.507	0.001	−0.491	0.002
Baseline systolic blood pressure	0.132	0.428	−0.536	<0.001
Peak systolic blood pressure	0.470	0.003	−0.646	<0.001
Cardiac catheterization				
LV ejection fraction	0.211	0.204	−0.277	0.092
LV end-diastolic pressure	−0.097	0.564	0.304	0.063
LV end-diastolic volume	−0.070	0.677	0.419	0.009
Cardiac index	0.347	0.033	−0.493	0.002
PAWP	−0.342	0.036	0.276	0.093
Systolic PA pressure	−0.353	0.030	0.364	0.025
LV dP/dt_{max} at baseline	0.286	0.081	−0.557	<0.001
LV dP/dt_{max} (5 μg kg^{-1} min^{-1})	0.339	0.037	−0.388	0.016
LV dP/dt_{max} (10 μg kg^{-1} min^{-1})	0.428	0.007	−0.355	0.029
LV dP/dt_{max} (15 μg kg^{-1} min^{-1})	0.490	0.002	−0.395	0.014

CPX = cardiopulmonary exercise testing; peak VO_2 = peak oxygen uptake; VE/VCO_2 slope = the minute ventilation/carbon dioxide production; GFR = glomerular filtration rate; BNP = brain natriuretic peptide; LV = left ventricular; E/Ea ratio = ratio of early transmitral flow velocity to early diastolic mitral annular velocity; PAWP = pulmonary arterial wedge pressure; PA = pulmonary artery; LV dP/dt_{max} = maximal first derivative of left ventricular pressure.

Dobutamine is a direct β-agonist that has been used to evaluate myocardial contractile reserve in chronic HF [31]. Few studies have evaluated the adrenergic contractile response to dobutamine infusion by measurement of the increase in LV dP/dt_{max} in patients with non-ischemic LV systolic dysfunction [32,33]. Several studies based on dobutamine stress echocardiography have shown a relationship between prognosis and adrenergic myocardial contractile reserve, as determined by measurement of LV systolic function indices such as LVEF or cardiac output [10,34]. However, many investigations which reported DST were measured by echocardiography [10,11]; here, we more accurately evaluated dobutamine response by measuring using catheterization with a high-fidelity micromanometer.

Decreased response to dobutamine infusion is a marker of the pathological status of myocardial damage and is closely associated with impaired peak VO_2 [27]. In the present study, peak VO_2 was significantly correlated with the absolute value of LV dP/dt_{max} and more strongly correlated with ΔLV dP/dt_{max}. Peak VO_2 was also independently correlated with ΔLV dP/dt_{max} and plasma BNP level. On the other hand, VE/VCO_2 slope was not correlated with ΔLV dP/dt_{max}. Because the percentage increase in LV dP/dt_{max} induced by dobutamine is especially unaffected by factors such as peripheral ergoreceptor activation, hyperventilation, and LV dP/dt_{max} at baseline, it is thought to be a useful and direct assessment of myocardial contractile reserve. Therefore, the results of this study suggest that myocardial contractile reserve may be strong determinant for peak VO_2, but not VE/VCO_2 slope in our study population. Furthermore, VE/VCO_2 slope was strongly correlated with plasma BNP level. The abnormal ventilatory response to exercise seems to be related to sympathetic activation, renin–angiotensin system [35] and ergoreflex activation [36] rather than to myocardial contractile reserve.

Our group reported previously that DST is a useful diagnostic tool for identifying reduced adrenergic contractile reserve related to altered myocardial expression of the β_1-adrenergic receptor and Ca^{2+}-handling mRNA level, even in asymptomatic or mildly symptomatic patients with IDCM [27]. A direct relationship of the degree of β_1-receptor down-regulation to peak VO_2 was also found in patients with IDCM [37]. These results suggest that decreased peak VO_2 is potentially related to impaired Ca^{2+}-handling or β_1-adrenergic receptor in patients with IDCM.

Myocardial contractile reserve, as determined by dobutamine stress echocardiography, predicts improvement in LVEF with β-blocker therapy [29]. In the absence of contractile reserve (i.e., when myocytes have been supplanted by replacement fibrosis because of cell death and interstitial remodeling), ventricular function cannot be improved by this biological mechanism because there are not enough contractile units. Contractile reserve itself appears to improve after LVEF has increased with β-blocker therapy. Thus, the benefit of β-blockade in HF patients is related not only to improvement in resting ventricular function but also to improved contractile reserve and the ability to respond to stress, likely to be found during exercise. However, we did not measure contractile reserve after β-blocker therapy. Higher peak VO_2 might indicate higher contractile reserve, and therefore a better potential response to β-blocker therapy and improved prognosis.

CPX is a useful tool for assessment of exercise tolerance and therapeutic effects in patients with HF, and accurate and repetitive measurements are available to the clinician at a reasonable cost. Indeed,

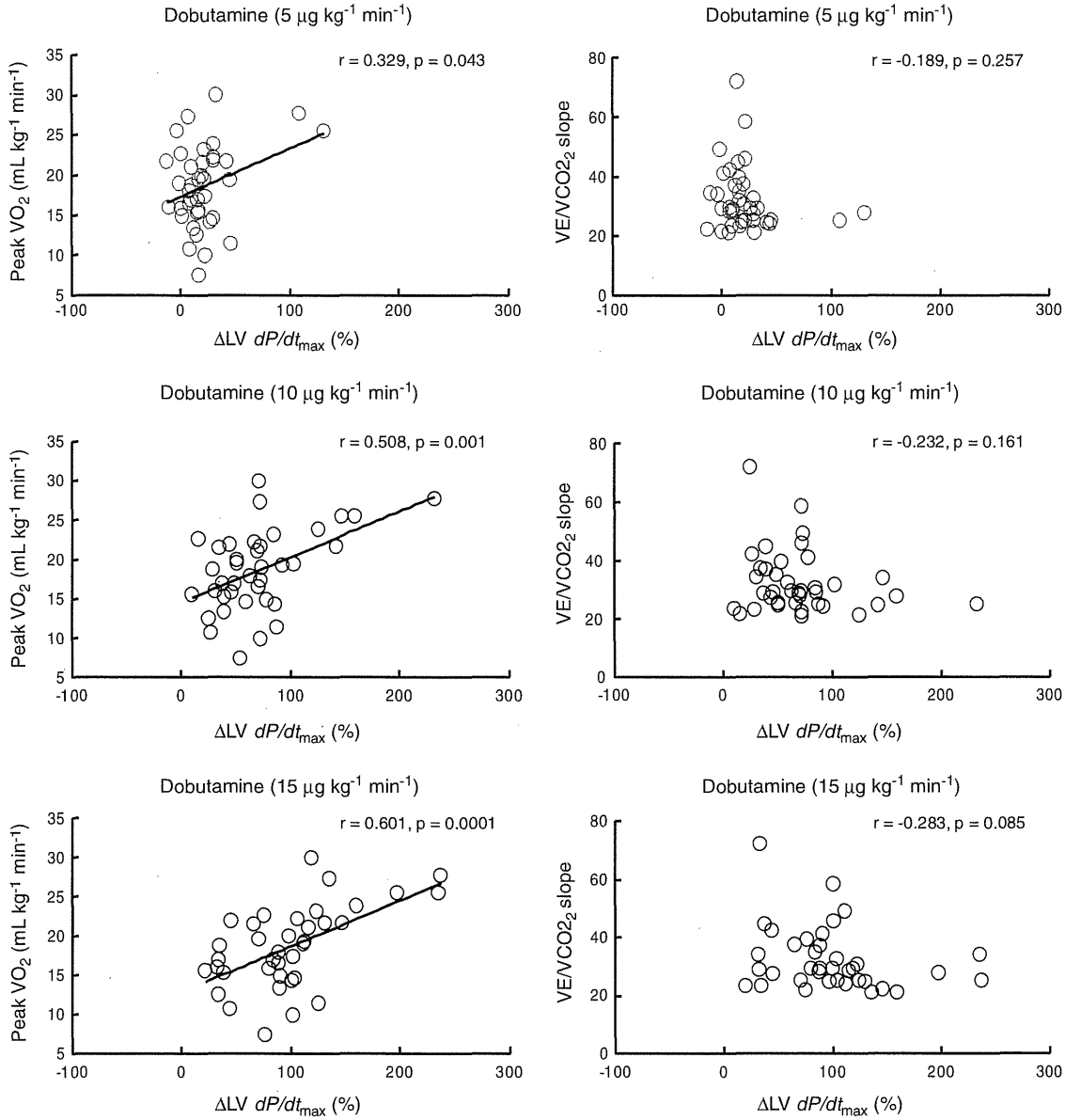

Fig. 2. Correlation between myocardial contractile reserve and peak VO_2, VE/VCO_2 slope. ΔLV dP/dt_{max} was significantly correlated with peak VO_2, and the correlation became more pronounced as the dose of dobutamine was increased. In contrast, no significant inverse correlation between ΔLV dP/dt_{max} and VE/VCO_2 slope was apparent, even at the maximum dose of dobutamine. ΔLV dP/dt_{max} is the percentage increase in LV dP/dt_{max} induced by dobutamine, and this index was defined on the basis of the formula: ΔLV dP/dt_{max} (x) (%) = [LV dP/dt_{max} (x) − LV dP/dt_{max} (baseline)] / LV dP/dt_{max} (baseline), where x = the dose of dobutamine (μg kg^{-1} min^{-1}).

especially for the observation of cardiac deterioration in patients with known IDCM, peak VO_2 possibly provide meaningful clinical information as a surrogate for cardiac reserve. Given the results of this study, peak VO_2 can represent myocardial contractile reserve, indicating that preserved systolic contractile reserve may be a feature in relatively mild degree of heart failure, in ambulatory patients with IDCM.

There are several limitations in our study. First, this study was performed in a small number of patients. Second, as regards to medication,

Table 5
Multivariate regression analysis of CPX variables.

Parameter	Peak VO_2			VE/VCO_2 slope		
	β	(95% CI)	p-value	β	(95% CI)	p-value
ΔLV dP/dt_{max} (10 μg kg^{-1} min^{-1})	0.430	(0.012–0.086)	0.011	0.052	(−0.054–0.079)	0.708
BNP	−0.421	(−0.017–−0.002)	0.010	0.813	(0.026–0.052)	<0.001
LVEF	−0.251	(−0.288–0.039)	0.131	0.064	(−0.228–0.362)	0.648
E/Ea ratio	−0.183	(−0.272–0.059)	0.201	0.001	(−0.299–0.301)	0.995

CPX = cardiopulmonary exercise testing; peak VO_2 = peak oxygen uptake; VE/VCO_2 slope = minute ventilation/carbon dioxide production; LV dP/dt_{max} = maximum first derivative of left ventricular pressure; ΔLV dP/dt_{max} = percentage increase in LV dP/dt_{max} induced by dobutamine; BNP = brain natriuretic peptide; LVEF = left ventricular ejection fraction; E/Ea ratio = ratio of early transmitral flow velocity to early diastolic mitral annular velocity; CI = confidence interval.

especially patients on β-blocking agents, therapy was kept unchanged. This may have resulted in some false-negative results in DST. However, the optimum dose of dobutamine to assess contractility is not defined, and it did not appear ethical to withhold a lifesaving therapy. Third, the assessment of peripheral factors was not checked. The patients in the present study had a mean of peak VO_2 of 18.6 mL kg^{-1} min^{-1}, which was relatively preserved exercise tolerance in IDCM patients. Because all subjects in this study were ambulatory and in stable condition, with normal respiratory function and relatively mild symptoms, the influence of lung and peripheral factors on VO_2 might be minimum.

In conclusion, based on DST findings, we suggest that peak VO_2, but not VE/VCO_2 slope, reflects myocardial contractile reserve. The findings of our study may provide evidence to differentiate pathophysiological insights between peak VO_2 and VE/VCO_2 slope, major prognostic CPX parameters. Further research could be designed to observe time course of deterioration of cardiac reserve by peak VO_2 as a surrogate marker. Further studies with larger numbers of patients, including those with more severe HF symptoms, are needed before our results can be applied more generally to IDCM patients with HF.

Funding

The work was supported in part by the Ministry of Education, Culture, Sports, Science and Technology of Japan [grant number 21790716 to A.H.].

Acknowledgements

The authors of this manuscript have certified that they comply with the Principles of Ethical Publishing in the International Journal of Cardiology.

References

[1] Jessup M, Brozena S. Heart failure. N Engl J Med 2003;348:2007–18.
[2] Myers J, Prakash M, Froelicher V, Do D, Partington S, Atwood JE. Exercise capacity and mortality among men referred for exercise testing. N Engl J Med 2002;346:793–801.
[3] Wroblewski H, Kastrup J, Mortensen SA, Haunso S. Abnormal baroreceptor-mediated vasodilation of the peripheral circulation in congestive heart failure secondary to idiopathic dilated cardiomyopathy. Circulation 1993;87:849–56.
[4] McBride BF, White CM. Anemia management in heart failure: a thick review of thin data. Pharmacotherapy 2004;24:757–67.
[5] O'Neill JO, Young JB, Pothier CE, Lauer MS. Peak oxygen consumption as a predictor of death in patients with heart failure receiving beta-blockers. Circulation 2005;111:2313–8.
[6] Guazzi M, Myers J, Peberdy MA, et al. Echocardiography with Tissue Doppler Imaging and cardiopulmonary exercise testing in patients with heart failure: a correlative and prognostic analysis. Int J Cardiol 2010;143:323–9.
[7] Corra U, Mezzani A, Bosimini E, Scapellato F, Imparato A, Giannuzzi P. Ventilatory response to exercise improves risk stratification in patients with chronic heart failure and intermediate functional capacity. Am Heart J 2002;143:418–26.
[8] Dickstein K, Cohen-Solal A, Filippatos G, et al. ESC Guidelines for the diagnosis and treatment of acute and chronic heart failure 2008: the Task Force for the Diagnosis and Treatment of Acute and Chronic Heart Failure 2008 of the European Society of Cardiology. Developed in collaboration with the Heart Failure Association of the ESC (HFA) and endorsed by the European Society of Intensive Care Medicine (ESICM). Eur Heart J 2008;29:2388–442.
[9] Jessup M, Abraham WT, Casey DE, et al. 2009 focused update: ACCF/AHA Guidelines for the Diagnosis and Management of Heart Failure in Adults: a report of the American College of Cardiology Foundation/American Heart Association Task Force on Practice Guidelines: developed in collaboration with the International Society for Heart and Lung Transplantation. Circulation 2009;119:1977–2016.
[10] Scrutinio D, Napoli V, Passantino A, Ricci A, Lagioia R, Rizzon P. Low-dose dobutamine responsiveness in idiopathic dilated cardiomyopathy: relation to exercise capacity and clinical outcome. Eur Heart J 2000;21:927–34.
[11] Paraskevaidis IA, Adamopoulos S, Kremastinos DT. Dobutamine echocardiographic study in patients with nonischemic dilated cardiomyopathy and prognostically borderline values of peak exercise oxygen consumption: 18-month follow-up study. J Am Coll Cardiol 2001;37:1685–91.
[12] Natali R, Lotrionte M, Marchese N, et al. Prediction of functional capacity by low-dose dobutamine stress echocardiography in chronic heart failure. Minerva Cardioangiol 2008;56:277–85.
[13] Paraskevaidis IA, Tsiapras DP, Adamopoulos S, Kremastinos DT. Assessment of the functional status of heart failure in non ischemic dilated cardiomyopathy: an echo-dobutamine study. Cardiovasc Res 1999;43:58–66.
[14] Chua TP, Clark AL, Amadi AA, Coats AJ. Relation between chemosensitivity and the ventilatory response to exercise in chronic heart failure. J Am Coll Cardiol 1996;27:650–7.
[15] Griffin BP, Shah PK, Ferguson J, Rubin SA. Incremental prognostic value of exercise hemodynamic variables in chronic congestive heart failure secondary to coronary artery disease or to dilated cardiomyopathy. Am J Cardiol 1991;67:848–53.
[16] Hunt SA, Abraham WT, Chin MH, et al. ACC/AHA 2005 Guideline Update for the Diagnosis and Management of Chronic Heart Failure in the Adult: a report of the American College of Cardiology/American Heart Association Task Force on Practice Guidelines (Writing Committee to Update the 2001 Guidelines for the Evaluation and Management of Heart Failure): developed in collaboration with the American College of Chest Physicians and the International Society for Heart and Lung Transplantation: endorsed by the Heart Rhythm Society. Circulation 2005;112:e154–235.
[17] Richardson P, McKenna W, Bristow M, et al. Report of the 1995 World Health Organization/International Society and Federation of Cardiology Task Force on the Definition and Classification of cardiomyopathies. Circulation 1996;93:841–2.
[18] Matsuo S, Imai E, Horio M, et al. Revised equations for estimated GFR from serum creatinine in Japan. Am J Kidney Dis 2009;53:982–92.
[19] Cheitlin MD, Armstrong WF, Aurigemma GP, et al. ACC/AHA/ASE 2003 guideline update for the clinical application of echocardiography—summary article: a report of the American College of Cardiology/American Heart Association Task Force on Practice Guidelines (ACC/AHA/ASE Committee to Update the 1997 Guidelines for the Clinical Application of Echocardiography). J Am Coll Cardiol 2003;42:954–70.
[20] Lang RM, Bierig M, Devereux RB, et al. Recommendations for chamber quantification: a report from the American Society of Echocardiography's Guidelines and Standards Committee and the Chamber Quantification Writing Group, developed in conjunction with the European Association of Echocardiography, a branch of the European Society of Cardiology. J Am Soc Echocardiogr 2005;18:1440–63.
[21] Ommen SR, Nishimura RA, Appleton CP, et al. Clinical utility of Doppler echocardiography and tissue Doppler imaging in the estimation of left ventricular filling pressures: a comparative simultaneous Doppler-catheterization study. Circulation 2000;102:1788–94.
[22] ATS/ACCP. Statement on cardiopulmonary exercise testing. Am J Respir Crit Care Med 2003;167:211–77.
[23] Bard RL, Gillespie BW, Clarke NS, Egan TG, Nicklas JM. Determining the best ventilatory efficiency measure to predict mortality in patients with heart failure. J Heart Lung Transplant 2006;25:589–95.
[24] Wasserman K, Whipp BJ, Koyl SN, Beaver WL. Anaerobic threshold and respiratory gas exchange during exercise. J Appl Physiol 1973;35:236–43.
[25] Wasserman K, Beaver WL, Whipp BJ. Gas exchange theory and the lactic acidosis (anaerobic) threshold. Circulation 1990;81:II14–30.
[26] Somura F, Izawa H, Iwase M, et al. Reduced myocardial sarcoplasmic reticulum Ca(2+)-ATPase mRNA expression and biphasic force-frequency relations in patients with hypertrophic cardiomyopathy. Circulation 2001;104:658–63.
[27] Kobayashi M, Izawa H, Cheng XW, et al. Dobutamine stress testing as a diagnostic tool for evaluation of myocardial contractile reserve in asymptomatic or mildly symptomatic patients with dilated cardiomyopathy. JACC Cardiovasc Imaging 2008;1:718–26.
[28] Piepoli M, Clark AL, Volterrani M, Adamopoulos S, Sleight P, Coats AJ. Contribution of muscle afferents to the hemodynamic, autonomic, and ventilatory responses to exercise in patients with chronic heart failure: effects of physical training. Circulation 1996;93:940–52.
[29] Eichhorn EJ, Grayburn PA, Mayer SA, et al. Myocardial contractile reserve by dobutamine stress echocardiography predicts improvement in ejection fraction with beta-blockade in patients with heart failure: the Beta-Blocker Evaluation of Survival Trial (BEST). Circulation 2003;108:2336–41.
[30] Chua TP, Ponikowski P, Harrington D, et al. Clinical correlates and prognostic significance of the ventilatory response to exercise in chronic heart failure. J Am Coll Cardiol 1997;29:1585–90.
[31] Leier CV, Unverferth DV. Drugs five years later. Dobutamine. Ann Intern Med 1983;99:490–6.
[32] Fowler MB, Laser JA, Hopkins GL, Minobe W, Bristow MR. Assessment of the beta-adrenergic receptor pathway in the intact failing human heart: progressive receptor down-regulation and subsensitivity to agonist response. Circulation 1986;74:1290–302.
[33] Dubois-Rande JL, Merlet P, Roudot F, et al. Beta-adrenergic contractile reserve as a predictor of clinical outcome in patients with idiopathic dilated cardiomyopathy. Am Heart J 1992;124:679–85.
[34] Naqvi TZ, Goel RK, Forrester JS, Siegel RJ. Myocardial contractile reserve on dobutamine echocardiography predicts late spontaneous improvement in cardiac function in patients with recent onset idiopathic dilated cardiomyopathy. J Am Coll Cardiol 1999;34:1537–44.
[35] Passino C, Poletti R, Bramanti F, Prontera C, Clerico A, Emdin M. Neuro-hormonal activation predicts ventilatory response to exercise and functional capacity in patients with heart failure. Eur J Heart Fail 2006;8:46–53.
[36] Ponikowski PP, Chua TP, Francis DP, Capucci A, Coats AJ, Piepoli MF. Muscle ergoreceptor overactivity reflects deterioration in clinical status and cardiorespiratory reflex control in chronic heart failure. Circulation 2001;104:2324–30.
[37] White M, Yanowitz F, Gilbert EM, et al. Role of beta-adrenergic receptor down-regulation in the peak exercise response in patients with heart failure due to idiopathic dilated cardiomyopathy. Am J Cardiol 1995;76:1271–6.